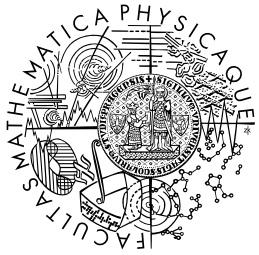

FACULTY
OF MATHEMATICS
AND PHYSICS
Charles University

MASTER THESIS

Bc. Veronika Červenková

Plasma methods for modification and preparation of biopolymers

Department of Macromolecular Physics

Supervisor of the master thesis: Daniil Nikitin, Ph.D.

Study programme: Physics of Condensed Matter and Materials

Study branch: Polymer physics

Prague 2023

I declare that I carried out this master thesis independently, and only with the cited sources, literature and other professional sources. It has not been used to obtain another or the same degree.

I understand that my work relates to the rights and obligations under the Act No. 121/2000 Sb., the Copyright Act, as amended, in particular the fact that the Charles University has the right to conclude a license agreement on the use of this work as a school work pursuant to Section 60 subsection 1 of the Copyright Act.

In ..... date ....

Author's signature

Acknowledgments

I would like to express my gratitude to people who helped and supported me during the Master's study. Firstly, I am deeply thankful to my supervisor Daniil Nikitin, Ph.D. for a kind approach, patient listening, great responsiveness and sharing of valuable knowledge and experience during my experimental work. I would like to extend my sincere thanks to prof. Ing. Andrey Shukurov, Ph.D. for guidance and advice during the thesis formation. I could not have completed my thesis without the help of other members of the department, especially Doc. RNDr. Lenka Hanyková, Dr. and doc. RNDr. Ivan Krakovský, CSc. Finally, I am very grateful to Bc. Lenka Doudová, Mgr. Hana Mašková, and RNDr. Ján Štěrba, Ph.D. from the Department of chemistry, University of South Bohemia in České Budějovice, for their pleasant and prompt attitude and for experiments that raised this thesis to next scientific level.

Title: Plasma methods for modification and preparation of biopolymers

Author: Bc. Veronika Červenková

Department: Department of Macromolecular Physics

Supervisor: Daniil Nikitin, Ph.D., Department of Macromolecular Physics

Abstract: The thesis covers the main results of research on atmospheric pressure plasma modification of biopolymers for the preparation of functional materials. Sodium alginate solutions processed by means of a plasma jet were successfully used for the casting of foils with advanced mechanical properties. It was observed that alginate's final performance does not only depend on the originating biopolymer viscosity but is significantly influenced by the type of working gas used for plasma modification. The antibacterial effect of alginate foils incorporated with almond essential oil was demonstrated as a promising extension of alginate's application in food storage. The results of plasma-initiated degradation of high-molecular-weight chitosan were studied in terms of its water-solubility. The analysis of structural properties demonstrated deep destruction of chitosan including the fragmentation of low-molecular-weight oligomers presented in the control sample. The fraction perfectly soluble in water was obtained using plasma processing as was demonstrated by NMR. The plasma solution system was demonstrated to be a suitable tool for enhancing chitosan's degradation for a possible application in crop protection.

Keywords: atmospheric pressure plasma, biopolymers

Contents

Introduction

Living in a modern consumer society has countless privileges. However, innovations and trends keep raising global demands. Environmental pollution by conventional synthetic polymers has been recognized as one of the major problems. The main drawback of plastic use is its insufficient processing: more than half of plastic waste becomes thrown into the environment. The extremely slow degradability of conventional polymers and the toxicity of their residuals pose a serious threat to many ecosystems inhabiting our planet. Among all strategies aimed to solve this problem, materials stemming from renewable resources could represent a promising alternative to conventional plastics.

Biopolymers derived from living organisms (such as starch, proteins, cellulose, chitin, chitosan, and alginate) are the major source for the development of advanced polymeric materials to replace petrochemicals in many industrial applications. They are gaining increasing attention in the scientific community due to their unique properties (non-toxicity, biocompatibility, biodegradability) and great application potential (e.g., in biocatalysis, medicine, and the food industry). However, compared to synthetic polymers, biopolymers are sometimes incompatible with traditional processing technologies and demonstrate inferior performances in terms of functional and structural properties [1].

Among different novel approaches for polymer processing, non-thermal plasma is successfully used for the improvement of biopolymers' functionality and properties. Unlike traditional wet chemical techniques, atmospheric pressure plasma-based methods eliminate the toxic solvent usage, are biocompatible, uniform in treatment, and suitable for heat-sensitive components. As a source of many active species, atmospheric-pressure plasma promotes biopolymer activation, fragmentation, and re-polymerization, which may be beneficial for obtaining new materials with desired characteristics.

This work aims to investigate the influence of plasma at atmospheric pressure on the chemical composition, structure, and functional properties of selected biopolymers. The research has been done on sodium alginate and chitosan, which were processed separately by different plasma sources and subsequently characterized by focusing on different properties.

The plasma processing of sodium alginate was motivated by two main applications:

1. promoting biopolymer crosslinking improves the functional properties of films with the the perspective of use for food packaging;

2. impregnating essential oil as a nature-derived antibacterial agent to produce novel bactericidal material for potential use in bio-medicine (e.g., for wound healing) as well as for the short-term storage of biological substances.

The sodium alginate was processed in form of an aqueous solution via an atmospheric pressure plasma jet ignited in Ar and Ar/air mixture. The plasma-treated solution was further used for the casting of biodegradable foils. Both solutions and foils were characterized regarding their mechanical, structural, and composition properties as well as metabolic activity.

The main drawback of chitosan lies in its poor water solubility making problematic its application as a natural fertilizer. Therefore, the solution of high molecular weight chitosan was processed using DC glow discharge with a liquid cathode to obtain lower-molecular-weight oligomers possessing solubility in water. The plasma-initiated degradation of chitosan without violation of its chemical structure was successfully confirmed.

1. Theoretical part

1.1 Plastics and processing

The excessive use of conventional plastics in our society is currently attracting worldwide attention. Due to their remarkable properties such as elasticity, thermal stability, and durability, they are applied in different fields of industry, including packaging, clothing, building and construction, aerospace, and transportation.

Plastics have become ubiquitous. According to statistics, global plastic production has risen from 1.5 Mmt in 1950 to 367 Mmt in 2020 [2] from which 21.3% has been recycled, 21.8% incinerated, yet the vast majority (53.8%) disposed [3]. The idea of plastic recycling has been believed to solve the waste crisis. However, not all plastic materials are suitable for undergoing the recycling process. In addition, manufactured plastics used in fast-moving consumer goods are often difficult to be recycled due to the multi-material multilayer plastic packaging techniques [4]. The latter often discourages consumers in many steps involved in the process. Therefore, incineration and landfill are thus the two most common methods used for plastic waste treatment. With toxicity caused by the ash and long-term degradation, neither of the methods suits the sustainable scenario.

Plastic degradation is particularly controversial. The poor degradability of plastics improves their material performance but threatens the environment by causing water and soil contamination ([5], [6]), harming wildlife [5] and even human health ([7], [8]). The majority of conventional plastics physically mill into smaller particles, so-called microplastics ($< 5\,\text{mm}$), representing a threat to marine ecosystems [9]. Plant growth and photosynthesis [10], mortality increase by ingestion ([11], [12]), and impact on the reproductive system of marine organisms [13] are a few examples of bulk plastic and microplastic adversity. Especially when it comes to *white pollution*, solid waste from petroleum-based synthetic polymers, such as polyethylene (PE), polypropylene (PP), polystyrene (PS), polyvinyl chloride (PVC), or polyethylene terephthalate (PET) used for packaging bags, tableware, plastic bottles, pipes, etc. In 2018, packaging accounted for 46% of global waste generation, being the main source of waste pollutants [14]. Table 1.1 summarizes the chemical structure and estimated half-life of the most common petrochemical plastics used in the packaging industry.

Society thus faces the most complex environmental crisis of the human era. A reconsideration of the "single-use" lifestyle is inevitable. Published by the European Commission, one of the key areas in need of research and innovation toward sustainable development [15] includes

> *innovation in new materials to replace traditional plastics (e.g., biodegradable plastics).*

A simple proposition opens up by finding a substitute with attractive and functional properties.

Polymer type	Chemical structure	Estimated half-life (y)	
		Land	Marine
HDPE	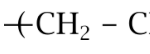	250	58
PP		780[a]	53
PS		> 2500[b]	-
PVC	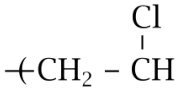	> 2500[b]	-
PET	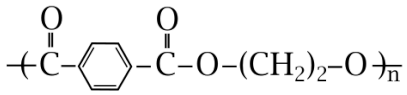	> 2500[b]	2.3[a]

Table 1.1: Structural formulae of conventional petrochemical polymers and estimated half-life (adapted from [16]). Half-life refers to converting the first 50% of the polymer mass.

[a]Corresponds to data collected in the presence of a degradation accelerator and/or for plastics containing a rapidly degrading filler. [b]The value indicated that the relevant studies detected no measurable degradation, possibly due to the duration of the experiment being too short, allowing only an estimated lower limit for the extrapolated degradation time.

1.2 Biopolymers

Biopolymers, or natural biodegradable polymers, are long-chained well-defined macromolecules synthesized in plants and living organisms due to complex metabolic processes. With their unique properties such as biodegradability, biocompatibility, non-toxicity, and abundance in nature, biopolymers have garnered interest both in academia and industry. They prove application in drug delivery ([17],[18]), food packaging ([19],[20],[21]) wound dressing ([22],[23]), tissue engineering ([24],[25]), wastewater treatment ([26],[27]) or agrotechnology ([28],[29]).

Typical examples of biopolymers are proteins, such as collagen embodied in connective tissues or its derivative gelatin. Cellulose, chemically extracted from the cell walls of cotton, wood, and some herbaceous plants is the most abundant biodegradable polymer on the Earth. As a well-known carbohydrate extracted from agricultural plants, starch has become one of the cheapest biopolymers receiving considerable attention for starch-based composites [30]. Chitin and its derivatives can be found in the exoskeleton of crustaceans, whereas alginate is mainly found in red, brown, and some green algae. Bacterial polyesters, such as PHB (polyhydroxybutyrate) or PHBV (polyhydroxybutyrate-valerate), are produced by a wide range of bacteria as reserve materials for carbon and energy. Several studies have also confirmed the benefits of other existing natural biodegradable polymers, including elastin [31], fibrin [32], or hyaluronate [33].

Biopolymers come under a large group of materials called biodegradable poly-

mers. The term *degradable* indicates the ability of the polymer to be decomposed by the action of enzymes and/or chemicals with living organisms (bacteria, fungi, or yeast) [34]. The classification of biodegradable polymers slightly differs across literature depending upon the origin or the synthesis method. In general, biodegradable polymers can be either natural or synthetic. Depending on their degradation mode, they can be further classified as hydrolytically or enzymatically degradable. Upon their origin, they can be derived from petrochemical or renewable sources. Figure 1.1 refers to the classification of biodegradable polymers based on their evolution (from left to right): 1) obtained from biomass, 2) obtained from petrochemical resources, 3) obtained from microbial production, and 4) conventionally and chemically synthesized [35]. Biomass and micro-organisms products should be considered natural biopolymers.

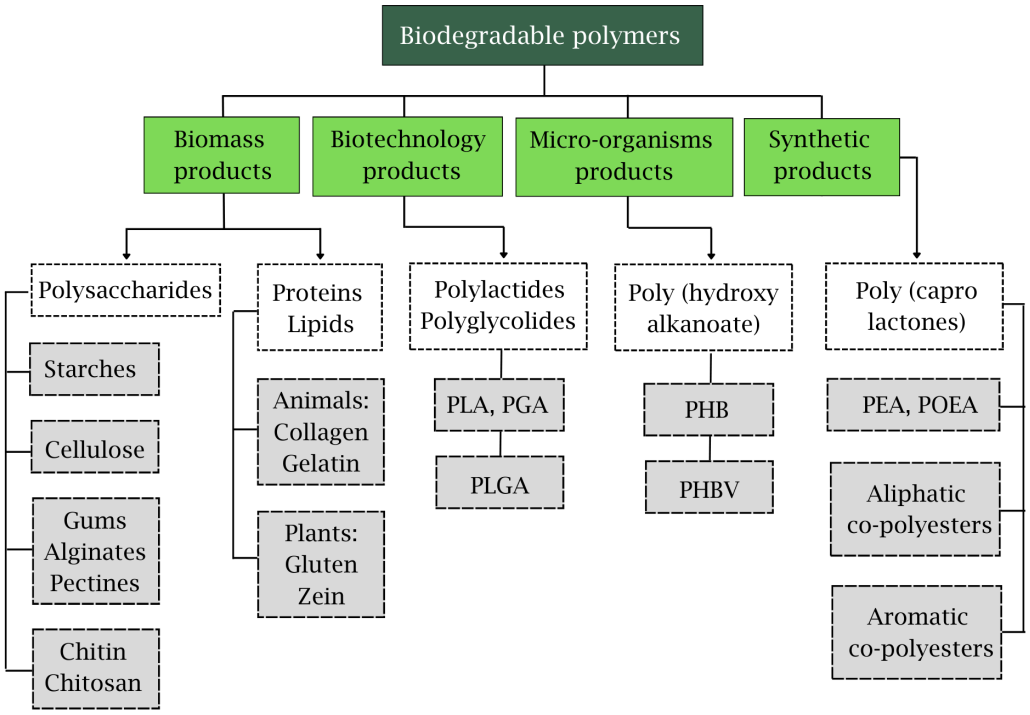

Figure 1.1: Classification of biodegradable polymers, adapted from [35].

Although synthetic biopolymers do not follow the objective of this study, we shall make a brief discussion on their basic properties and recent applications. Even though the association of *synthetic* and *biodegradable* may seem paradoxical, polymers with hydrolyzable backbones have been found to be susceptible to biodegradation [16]. Poly(α-esters), poly(capro lactones), poly(ester amides) (PEA), polyurhetanes, and polyanhydrides are hydrolitically degradable polymers comprising labile chemical linkages.

From the class of poly(α-esters), the most extensively investigated polymers are PGA (polyglycolic acid), PLA (polylactic acid), and their copolymer PLGA. Glycolic acid naturally occurs in certain fruits, beets, and sugarcane, whereas lactic acid can be found either in living organisms or synthesized by the microbial fermentation of agricultural by-products (mostly carbohydrates). PLA meets many requirements in the packaging industry. When plasticized with its

monomers, PLA becomes increasingly flexible, imitating the performance of conventional polymers [36]. Replacing standard plastic in service ware, PLA has been commercially fabricated for the use of yogurt cups [37], single-use hot beverage cups [38] or grocery bags [39]. On the other hand, PGA is a highly crystalline biopolymer with great mechanical and barrier properties but low solubility in organic solvents [40]. Several studies have proven PGA's fine properties, mainly in the field of tissue engineering [41] and bone fixation [42].

Poly(capro lactones) are semi-crystalline, hydrophobic polymers thoroughly studied in controlled-release systems for drug delivery [43]. However, a high degree of crystallinity and hydrophobicity decelerates the degradation process, and thus, PCL is less biocompatible with soft tissue [35]. A modification of PCL with poly(ethylene glycol) (PEG), a hydrophilic and non-toxic polymer, is often proposed to enhance thermosensitive properties of the prior [44].

The second large group of synthetic biomaterials comprises polymers with carbon backbones. Vinyl polymers, such as poly(vinyl alcohol) (PVA), are readily degraded in wastewater-activated sludges but compared to the hydrolyzable polymers, the initial biodegradation step requires an oxidation process [35]. Recently, significant progress has been made to enhance the properties of polymeric hydrogel membranes for wound dressing applications by using PVA-based hydrogel dressings [45].

1.2.1 Chitosan

Chitosan is a natural amino polysaccharide derived from chitin, a crystalline biopolymer found in the exoskeleton of crustaceans and arthropods or the cell wall of fungi and yeast [46]. As plants produce cellulose in their cell walls, similarly, insects and crustaceans produce chitin in their shells [47]. Considering the amount of its annual production, chitin has become the most abundant polymer in nature after cellulose.

Chitosan, β-1,4-D-glucosamine, is the most important derivative of chitin. During chitin's extraction from shells, a small amount of deacetylation might occur, leaving amino groups in the chitin's ring structure [48]. This makes chitin a copolymer composed of N-acetyl-β-D-glucosamine units linked through 1,4-glycosidic bonds, see fig. 1.2. Chitosan is obtained by chitin's (partial) deacetylation in the solid state under alkaline conditions, typically using NaOH, or by enzymatic hydrolysis in the presence of a chitin deacetylase [46]. During this process, a defined percentage of acetylated units is dissociated from the copolymer's structure leading to a significant change in the biopolymer's properties. Consequently, the molar ratio of D-glucosamine units, the degree of deacetylation (DD), has often been cited as an important parameter determining chitosan's physiochemical and biological properties such as crystallinity, hydrophilicity, degradation, and cell response [49].

Depending on the initial conditions, different DD might be obtained. The DD of most commercial chitosan varies between 70% and 90% [50]. The properties of chitosan depend not only on DD, but molecular weight, the distribution of G and A-blocks along the main chain, and the purity of the product [51]. With desirable structural modifications, chitosan has immense commercial potential, especially in biomedical applications and cosmetology. Hydrogels, films, coatings, fibers,

and sponges, are only a few examples of chitosan practical utilization.

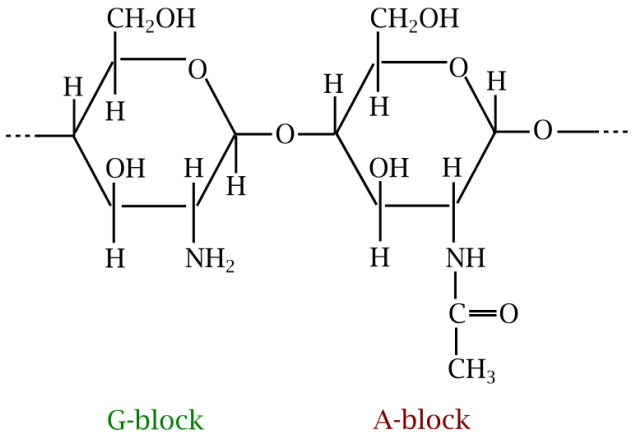

Figure 1.2: Structure of chitin and chitosan. As a matter of scale, the resulting product depends only on the molar fraction of blocks in the main chain: chitin contains $> 50\%$ A-blocks, whereas chitosan contains $> 50\%$ G-blocks [48].

While chitin is insoluble in most organic solvents, chitosan is soluble in dilute acids (1% (v/v) acetic acid is a commonly used solvent) [52]. The necessity of the use of acids for chitosan dissolution is unfavorable for some applications including food packaging and agriculture. A large emphasis has been made to fabricate water-soluble chitosan as a natural additive (antibacterial agent) or coating (release controller) of fertilizers. Low-molecular-weight chitosan exhibits plant-protective properties against worms, fungi, viruses, and bacterial infections [53]. Improvement of the fertilizer's degradation rates and water retention capabilities are other examples of chitosan's enormous technological potential [54].

1.2.2 Sodium alginate

Alginate, a common term for alginic acid salt, is an anionic polysaccharide composed of uronic acid residues. As a natural biopolymer, alginate is typically extracted from the cell wall of brown algae by treatment with aqueous alkaline solutions [55]. After the addition of NaCl or $CaCl_2$ to alginate filtrate, treatment with dilute HCl enables salt transformation into alginic acid [56]. Further purification and conversion produce a light yellow sodium alginate powder forming a highly viscous aqueous solution ([51], [57]). Besides the algal sources, alginate can also be produced by microbial fermentation using specialized bacteria [58].

Similarly to chitosan, sodium alginate is a linear copolymer comprising $(1, 4)$-linked β-D-mannuronic and α-L-guluronic acid residues forming regions of M-blocks and G-blocks [35]. Illustrated in fig. 1.3, mannuronic and guluronic units are clearly conformational isomers. The ratio of the two uronic blocks and their sequential arrangements depends mainly on alginates' sources. For instance, different parts of *Laminaria hyperborea*, a species of the large brown alga, contain different amounts of the two acid residues (the leaves are abundant in mannuronic acid, whereas the stipe and the outer cortex contain a high amount of guluronic acid) [59]. The M/G ratio (in some way analogous to DD), as well as the sequence arrangement, plays a significant role in the polymeric performance. Alginic acids

rich in consecutive G-blocks (M/G < 1) exhibit higher water solubility than those rich in consecutive M-blocks [60]. Concerning solubility, pH is another parameter to be controlled. At low pH, alginates with more alternating MG blocks are soluble, whereas the consecutive block–rich alginates do not dissolve [61]. The mechanical properties of alginates are typically enhanced by increasing the length of G-blocks and molecular weight [56].

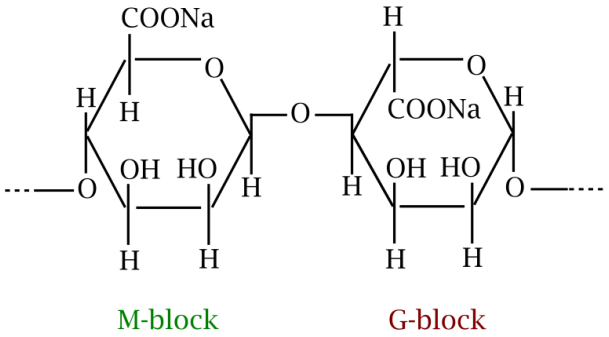

Figure 1.3: Structure of sodium alginate. M-block represents the mannuronate residue, G-block stands for the guluronate residue. Chain sequences are composed either of consecutive or alternating G and M-blocks.

As perspective biomaterials, alginates have been highly studied in the form of hydrogels. In solution, two G-blocks of adjacent polymer chains can cross-link with the introduction of Ca^{2+}([62], [57]). Besides gelation alginate has good film-forming properties, and has been widely used for preparing various membrane materials [63].

Regarding its functionality and physical properties, sodium alginate can be easily dissolved in water, compatible with most additive molecules, and miscible with several materials, including thickeners, sugars, fats, waxes, some surfactants, and some organic solvents (such as glycerin, propylene glycol, ethylene glycol, etc.) [57]. In addition, alginate evinces proven immunomodulatory [64], antioxidant [65] and inflammatory [66] effects. However, poor thermal stability, low mechanical and barrier properties, and incompatibility with heavy metals obstruct alginates from making a commercial breakthrough [59].

1.3 Essential oils

Foodborne illnesses originating from microbial contamination represent a major global problem. Opinions on the safety aspects of artificial food additives (benzoates, sorbates, acetic acid, potassium acetate, lactic acid, etc.) differ among academics and regulators specializing in food science, toxicology, and biology. Similarly, the use of pure or multi-metal nanoparticles has been questioned for their toxicity effects [67]. The negatively perceived chemical conservatives have challenged food industries to develop natural additives offering safer alternatives.

Essential oils (EOs) are one of the natural additives used in edible films and coatings in the food industry and in cosmetics (e.g., fragrances, creams, or body care products). EOs are complex mixtures of volatile compounds produced by living organisms [68]. For the use of commercial production, they are physically

isolated by pressing and distillation from a plant of known origin. Approximately 3000 EOs are known, of which about 300 are commercially important (destined primarily for the flavors and fragrances market) [69].

EOs have been extensively studied owing to their different biological properties and benefits for human health. It has been known that some EOs, such as almond, oregano, cinnamon, thyme, tea tree, etc., exhibit proven antimicrobial properties ([70],[71],[72],[73]). *Yen et al.* reported high antioxidant capacity of lemon balm extracted from *M. officinalis* as a potential antidiabetic agent [74]. Several EOs have also demonstrated anticancer and anti-inflammatory activity ([75], [76]).

Regarding the application, EOs can be added directly to the food or incorporated into the packaging material [77]. Films incorporated with EOs has been already tested on several foods such as octopus [78], ham [79], fish patties [80], or fresh beef [81]. However, no studies have yet been done on incorporating almond oil into sodium alginate films.

1.4 Plasma

1.4.1 Elementary processes

It has often been said that plasma is the fourth state of matter. Due to its definition, people usually refer to plasma in a gaseous state. From the view of thermodynamics, plasma may exist in the solid, liquid, or gaseous phases, and yet, with very unlike properties. The main difference between gas and plasma resides in the presence of free-charged particles, ions, and electrons, making plasma electrically conductive. More precisely, plasma is defined as

a quasi-neutral gas of charged and neutral particles which exhibits collective behavior [82].

A matter transforms to plasma with the continuous elevation of gas temperature. Temperature elevation boosts particles' energy, enhances their motion, and provokes collisions. When two neutral atoms collide, a charged particle can be created, a process called *ionization*. In non-thermal plasma, the electron impact ionization of gas neutrals represents the main channel to generate free-charged particles. For example, in argon plasma, high-energy electron interaction with atomic argon produces electrons and positive ions [83]

$$\mathrm{e}^- + \mathrm{Ar} \longrightarrow \mathrm{Ar}^+ + 2e^-, \tag{1.1}$$

or in the case of electronegative gases, electron capture may produce a stable negative ion [83]

$$\mathrm{e}^- + \mathrm{O}_2 \longrightarrow \mathrm{O}^- + \mathrm{O}. \tag{1.2}$$

As such, plasma can generate very high concentrations of energetic and chemically active species (e.g., excited and neutral atoms and molecules, ions, electrons, free radicals, metastables, and different wavelength photons), making plasma a highly demanded technological medium [84].

As the temperature rises, the collision frequency between neutral and charged particles increases. Unlike neutrals, charged species generate local concentrations of a positive or negative charge, which gives rise to electric fields. Simultaneously, their motion generates currents, and hence magnetic fields [82]. These fields exert electromagnetic forces on charged particles even at long distances. Therefore, plasma species undergo complex motion affected by local and further conditions and thus evince a "collective behavior". However, the density of ions and electrons remains the same ($n_i \approx n_e$) in all macroscopic volumes, which explains the term *quasi-neutral*.

Plasma can be found in nature during thunderstorms in lightning, in the ionosphere, and in space compassed in solar wind and stars, but it is also effectively man-made in a laboratory. When induced in laboratory conditions, plasma occurs in the form of electric discharge.

1.4.2 Plasma characteristics

Plasma can be characterized by the two most important parameters - the density n and the temperature T of plasma species.

The average kinetic energy of neutral particles, $E_k = \frac{1}{2}KT$ per degree of freedom [82], respects Maxwellian distribution with one characteristic temperature. Likewise, charged particles in plasma, i.e., heavy ions and light electrons, might have separate Maxwell's distributions with different temperatures T_i and T_e [82]. This leads to a non-equilibrium state and a rather complicated theory of plasma dynamics. Such "two-temperature" plasmas are typically found in gas discharges [85]. On the other hand, the solar plasma exists in an equilibrium state with $T_e \approx T_i$. Plasma temperature is often denoted in terms of energy KT_e[1] and varies from 10^{-1} to 10^6 eV [82].

Particle density n varies in a large range from 1 to $10^{30}\,\mathrm{m}^{-3}$. Solar wind near earth comprises particle density of $10^6\,\mathrm{m}^{-3}$, whereas the density of a custom laboratory plasma varies from 10^{16} to $10^{20}\,\mathrm{m}^{-3}$ [86]. Since charged particles control the heat transfer to the walls of plasma apparatus, laboratory discharges often require cooling systems.

As aforementioned, the existence of plasma is provided by several ionization processes. Plasma can be fully ionized, as in space, partially ionized, as in fluorescent lamps, or weekly ionized, as in low-pressure discharges, which contain many neutral atoms [85]. The degree of ionization α is thus defined as the molar fraction of the ion density n_i [87]

$$\alpha = \frac{n_i}{n_i + n_g}, \tag{1.3}$$

where n_g states the neutral gas density.

Plasma criteria

Another fundamental characteristic of plasma behavior is the ability of particles to shield out the applied electrostatic field, so-called the *Debye shielding* [82]. Let's consider an experiment in which a positively charged sphere is immersed in plasma containing ions and electrons. Eventually, the ions in the ball's proximity will be repelled, and the electrons will be attracted, leading to an altered local charge density. The potential $\varphi(r)$ of the ball after such a readjustment can be calculated as [88]

$$\varphi(r) = \frac{1}{4\pi\varepsilon_0}\frac{\exp(-r/\lambda_D)}{r}. \tag{1.4}$$

λ_D is the characteristic length scale known as the Debye length, proportional to $\sqrt{KT_e/n_e}$ [88]. The Debye length indicates the distance of the measurable potential of the ball (e.g., electrode or probe), or in other words, the distance over which a significant charge separation can occur. An ionized gas is considered plasma if n_e is high enough so that λ_D is much smaller than the system dimensions L, $\lambda_D \ll L$. In this case, whenever external potentials are introduced into the system, they are shielded in a region of length λ_D, leaving the bulk plasma free of external fields.

Debye shielding is a valid concept only with enough particles in the sheath region. The number of particles in the *Debye sphere* of radius λ_D is defined as [88]

[1] 1 eV is approximately equal to 11 605 K.

$$N_D = \frac{4\pi}{3} n_e \lambda_D^3. \tag{1.5}$$

To ensure the collective behavior of particles, plasma must satisfy the condition $N_D \gg 1$.

The second aspect of collective behavior is the time scale, after which a shielded equilibrium is established. This process involves lighter electrons rather than heavy ions. The electron plasma frequency ω_p, defined as [88]

$$\omega_p = \sqrt{\frac{e^2 n_e}{\varepsilon_0 m_e}}, \tag{1.6}$$

is the response rate to an external disturbance (e.g., electromagnetic waves or particle beams) at which electrons return to equilibrium. The time it would take plasma to adjust the insertion of the external field is denoted by τ_p, where $\tau_p = \omega_p^{-1}$. External electromagnetic waves of frequency ω lower than plasma frequency ω_p will be shielded, while waves of higher frequencies will propagate. A system can be considered a plasma if $\tau_p \ll \tau$, i.e. if $\omega_p \gg \omega$.

1.4.3 Plasma classification

Plasma can be classified according to different parameters. According to the thermodynamic equilibrium condition, equilibrium plasma can be generated at high pressures and temperatures. On the other hand, a non-equilibrium plasma (often termed thermal and cold) can be obtained at atmospheric pressure or lower with the temperature even close to ambient. The considered non-thermal plasma is exclusively associated with partially or weakly ionized plasma ($n_e \ll n_n$) with $\alpha = 10^{-4} - 10^{-6}$ [83]. Concerning the energy content, the plasma state can be classified as ideal (classical), non-ideal (degenerate), and relativistic [83].

Tab **??** summarizes types of plasma with respect to plasma temperature T, degree of ionization α, pressure p, defined as $p = nk_BT$, and applied generator field.

Parameter	Types of plasma		State
T	High-temperature	Thermal	$T_e \approx T_i \approx T_g = 10^6 - 10^8\,\mathrm{K}$
	Low-temperature	Cold[a]	$T_e \approx T_i \approx T_g \leq 2 \cdot 10^4\,\mathrm{K}$ $T_e \gg T_i \approx T_g = 300 - 10^3\,\mathrm{K}$
α	Fully ionized		$\alpha \approx 1$
	Partially ionized		$\alpha < 1$
	Weekly ionized		$\alpha \ll 1$
p	High-pressure		$p > 10^4\,\mathrm{Pa}$
	Low-pressure		$p < 10^2\,\mathrm{Pa}$
	Atmospheric		$p \approx 1\,\mathrm{bar}$
Plasma generators	Electrode-discharged		direct current (DC) alternating current (AC)
	Inductively-coupled		radio frequency (RF) microwave (MW)

Table 1.2: Classification of plasma according to different parameters based on [89].

[a] In literature, often called non-thermal.

1.4.4 Townsend mechanism of plasma generation

Let's consider a system of two (conductive) electrodes separated by a plane gap d of air at atmospheric pressure. If we increase voltage V on one of the electrodes (negatively charged cathode) concerning the second (positively charged anode), an electric field $E = \frac{V}{d}$ will arise in the gap. Primary electrons near the cathode provide low electric current I_0, drift to the anode, ionize the gas and generate avalanches described by the first Townsend ionization coefficient α [84]. Defined as the ratio of emitted electron flux to incoming ion flux [85], the first Townsend coefficient α is a function of reduced electric field strength E/p given by the empirical expression [90]

$$\alpha = pA \exp\left(\frac{-Bp}{E}\right), \tag{1.7}$$

where A and B are parameters depending on the gas type and electric field range. During the scattering process, primary electrons obtain random motion being accelerated or decelerated by the field, and produce positive ions moving to the cathode's surface, see fig. 1.4. Ions lead to the extraction of electrons due to the secondary electron emission from the cathode's surface. The secondary electron yield is described by the second Townsend coefficient γ [84].

The continuous energy loss from the primary electron collision processes (such as drift and diffusion to the walls) is, in fact, a severe loss to the system. Lost electrons have to be constantly replenished by the secondary electrons, i.e., by ion bombardment of the cathode's surface [91].

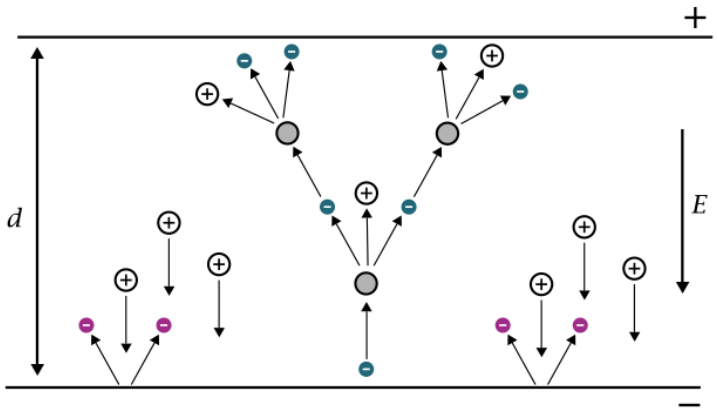

Figure 1.4: Electrical breakdown in a gap between two electrodes with an applied constant electric field, adapted from [84]. Primary electrons (blue) collide with neutral gas molecules (grey) and create positively charged ions (+) which reach the cathode's surface and generate secondary electrons (purple).

Total current I is thus a function of coefficients α, γ, primary electron current I_0, and the inter-electrode distance d, which leads to the Townsend formula [84]

$$I = \frac{I_0 \exp(\alpha d)}{1 - \gamma[\exp(\alpha d) - 1]}. \tag{1.8}$$

The Townsend breakdown mechanism occurs when the avalanche process can maintain itself. This can be expressed by the balance condition [85]

$$\gamma(\exp \alpha d - 1) = 1. \tag{1.9}$$

In this case, the denominator of eq. 1.8 approaches 0 (e.g., $I \to \infty$) and the transition to self-sustained current takes place. In this situation, secondary electron production at the cathode compensates for the loss of electrons at the anode [91]. By combining the Townsend formula (eq. 1.8) and the Townsend balance condition (eq. 1.9), we obtain Pashen's law: *the breakdown voltage V_b is a function of the product of pressure and distance between the electrodes* [87]. Represented by the *Paschen's curve* $V_b(pd)$, V_b increases linearly for large values of pd. For small pd there is a limiting value of pd below which breakdown cannot occur. The breakdown voltage acquires a minimum at some intermediate value of pd (depending on the combination of gas and cathode material).

1.4.5 Plasma discharges

Plasma discharges can be classified according to several parameters, including the current-voltage characteristics (fig. 1.5), the electrical breakdown mechanism, the type of the applied electric field, or the electron behavior [83]. Tab. 1.3 proposes a brief classification of the electric gas discharges according to the essential discharge processes: the electric breakdown mechanism and the electric power supplies.

Electrical processes	Types of discharges
Townsend mechanism	Townsend discharge Glow discharge Arc discharge
Streamer mechanism, micro discharges	Corona discharge Spark discharge Barrier discharge
Electrons in high-frequency electric field	Radio-frequency (RF) discharge Microwave (MW) discharge
Cyclotron motion, resonances, wave heating, ExB drift	Magnetised discharge

Table 1.3: A brief overview of electric plasma discharges according to the breakdown mechanism and the plasma generation, adapted from [83].

DC glow discharge

The self-sustained (i.e., the avalanche effect of electrons keeps the continuous production of ion species) continuous DC discharge with cold cathode is defined as the *glow discharge*, the best-known type of non-thermal discharge widely used in plasma physics [84]. The term "glow" comes from the fact that the discharge is characterized by the appearance of several zones with a complex pattern of dark spaces and luminous layers details of which can be found in [92].

Fig. 1.5 shows a schematic current-voltage characteristic of low-pressure DC discharge. The Townsend breakdown mechanism occurs in the cathode sheath, leading to the glow discharge ignition (IV, V), as described in the previous section.

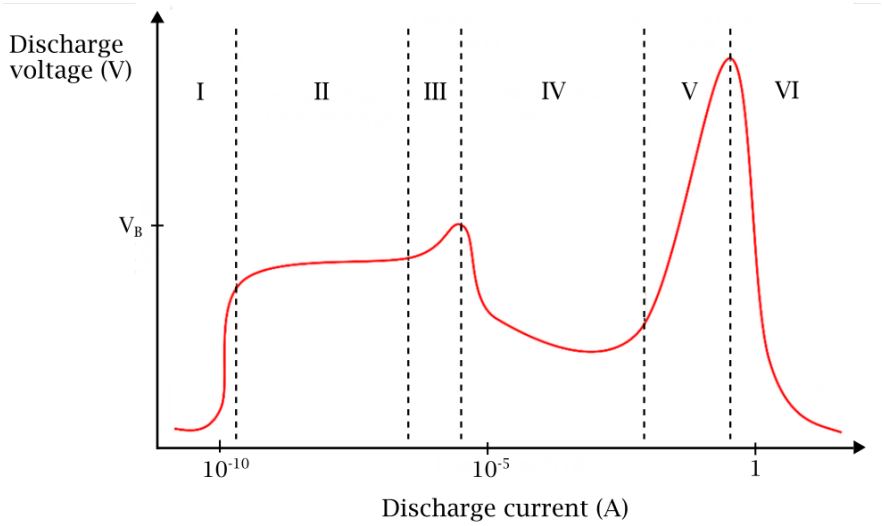

Figure 1.5: Generalized current-voltage characteristic of DC discharge for pressure in the range $10^1 - 10^3$ Pa, adapted from [93]. The curve can be divided into three main regions: 1) the Townsend regime (I-III) before spark ignition; 2) the glow regime consisting of "normal glow" (IV) and "abnormal glow" (V), and 3) arc regime (VI), where the plasma becomes highly conductive [94].

RF discharge

In RF discharges, the voltage breakdown mechanism is frequently-dependent showing minimum in the RF domain (20 kHz – 300 GHz), which is valid for a large range of pressures [95]. Compared to DC discharges, RF discharges are easier to ignite and can be operated at lower currents and power in the same pressure range, which reduces the risk for instabilities [95]. Accordingly, RF plasma sources have been encountered in research and technology with a large variety of discharge geometries. Among them, designs for specific applications led to the expansion of atmospheric-pressure RF plasma.

1.4.6 Atmospheric-pressure plasma

Atmospheric-pressure plasma is used in a variety of material and technological processes. Overcoming the drawbacks of vacuum operation, air-pressure systems may be suitable for various applications, including treating organic and inorganic surfaces (i.e., wool, seeds, cells, fabric, biopolymers, liquids, or synthetic polymers).

In air-pressure plasma, the mean free paths between electrons and ions are extremely short, which makes the generation mechanism collision dominated [96]. Under these conditions, air-pressure plasma may prevail in local thermodynamic equilibrium (LTE) [96]. LTE is satisfied in *thermal* plasma; however, in the case of *cold* atmospheric-pressure plasma, the electron temperature T_e acquires high values ($\sim$ units of eV), whereas the thermal motion of ions may be neglected. In cold air-pressure plasma, electrons and ions never achieve LTE [96]. The non-equilibrium state is possible since energy transfer from the applied electric field to the electrons is generally more efficient than the energy transfer from particle collisions [97]. To ensure thermal stability (minimization of gas heating and

arcing) with increasing pressure, some approaches have been developed, including the use of noble gases, cooling system, high gas flows, or reduced plasma size (increased surface-to-volume ratio) [97]. Furthermore, a high concentration of active species (i.e., reactive free radicals and excited state atoms) makes cold air-pressure plasma very reactive [96], a desirable property for surface modification.

Atmospheric-pressure plasma jet (APPJ) operated at RF mode is one of the most developed non-thermal discharge systems, which exhibits many characteristics of a conventional low-pressure glow discharge [98]. Generally, APPJ consists of two concentric electrodes through which flows one gas or a gas mixture. By applying RF power to the inner electrode, the gas discharge is ignited. The breakdown voltage V_b of APPJs varies from 50 to 200 V, being the only air-pressure source with V_b below that of low-pressure discharges [94]. The low injected power enables a stable discharge operation and avoids the arc transition [99]. Recently, APPJs have been effectively used in plasma medicine for disinfection and wound healing [100] as for the treatment of seeds [101], polymer foils [102] or cotton [103].

1.4.7 Solution plasma processing (SPP)

Atmospheric-pressure plasma has also adapted to the treatment of liquids. As a growing interdisciplinary area of research, solution plasma processing (SPP) has found applications in almost every scientific field. In the past, SPP has been mainly focused on wastewater treatment due to its ability to induce reactive species (such as OH radicals, superoxide anion O_2^-, and hydrogen peroxide H_2O_2) [104]. Nowadays, intensive progress has led to the synthesis and modification of various materials, such as metallic nanoparticles [105] or polymer foils [106].

There are several configurations of plasma-liquid systems. The electric discharge can be ignited in the gas phase above the liquid surface or directly in the liquid phase. The classification scheme of SPP systems based on the method of generation and configuration is as follows [107]:

1. Direct liquid phase discharges
2. Gas phase plasma producing reactivity in the liquid
   (a) Without direct contact/electrical coupling with the liquid
   (b) With direct contact/electrical coupling with the liquid (liquid electrode)
   (c) At the plasma-liquid interphase (surface discharges)
3. Multi-phase plasma
   (a) Gas phase plasma with dispersed liquid phase (aerosols)
   (b) Gas phase plasma dispersed in the gas phase (bubbles) in liquid

Among the various atmospheric-pressure plasma sources, a DC air glow discharge in contact with liquid has been a topic of the ongoing investigation. Glow discharge with a liquid electrode is a gas discharge excited between an external anode and an electrolyte surface, serving as a cathode. In this system, plasma is formed inside the liquid. APPJ is another option allowing plasma treatment of the liquid surface. In this case, the electric current does not flow directly through the solution. Plasma modification is reached via APPJ afterglow, and

the transfer of active species to liquid is ensured by convection and diffusion mechanisms [108].

1.4.8 Active species

The density of reactive species in non-equilibrium atmospheric-pressure plasma is crucial for understanding the interaction mechanism between plasma and treated surface. In particular, reactive oxygen and nitrogen species (RONS), e.g., NO, O_3, OH, H_2O_2, etc., are of deep interest since they are abundantly present or can easily be produced from ambient air.

In RF APPJs, primary reactive species are produced inside the discharge volume [109]. *Van Gessel et al.* studied the production of NO by APPJ operated with a mixture of argon and a varying amount of air, oxygen, and nitrogen. Nitrogen oxides are primarily formed by reacting N atoms with O_2. The NO density was found to increase with power and air concentration [110]. A measurable NO production was also recorded in the pure argon state due to the presence of ambient air. In another study by *Van Ham et al.*, the O_3 density in the effluent of APPJ was successfully promoted using argon with admixtures of air or oxygen. Similarly, O_3 density increases with increasing power and partial pressure of air mixed with the argon flow [111].

A major emphasis is drawn to APPJs, which are not in direct electrical contact with the liquid. Reactive species produced from the nozzle are transported to the liquid by the APPJ afterglow flow. Since the reactive flow is mainly devoid of ions, the liquid interaction is dominated by the neutral species produced by plasma and photolysis by UV photons generated in the plasma [107]. From the short-lived species, OH radical is a significant species produced by plasma interaction with liquid [107].

Regarding the formation of reactive species in solution, there is a significant difference in whether the plasma touches or not the surface of liquid [112]. *Kondeti et al.* studied different modes of the inactivation of bacteria due to reactive species produced by APPJ in/not in direct contact with the liquid surface [113]. The concentration of long-lived species (i.e., H_2O_2) in water solution generated by the Ar plasma decreases with the increasing liquid-nozzle distance. For the 4 mm liquid-nozzle distance, the pH of plasma-treated H_2O solution is significantly reduced to all plasma conditions. The short-lived species (i.e., $OH^{\bullet}$, O_2^{-}, $H^{\bullet}$) do not penetrate to the bottom of the treated solution; hence, they interact near the plasma-liquid interface. On the other hand, APPJ afterglow flow induces convection in the liquid. The convection recirculates the bacteria in the solution so that the surface replenishes with new bacteria during plasma treatment. Convection is thus an enhancing factor for the involvement of short-lived species in the bulk processes.

1.5 Plasma processes and polymers

Before discussing the formation of polymeric materials in plasma, so-called the *plasma polymerization*, a review of the fundamental aspects of polymerization is necessary.

There are two distinct mechanisms by which polymers are built up: *step* and *chain* polymerization. Their crucial difference lies in the nature of the species that can react with each other.

In step polymerization, a polymer is formed by the stepwise reaction between the functional groups of reactants with repetition [114]. The size of the polymer molecules slowly increases from monomer to dimer, trimer, tetramer, pentamer, etc.

$$M_{\mathrm{n}} + M_{\mathrm{m}} \longrightarrow M_{\mathrm{n+m}}. \tag{1.10}$$

As any two molecular species can react with each other, the monomer concentration quickly decreases. Long reaction times are necessary for high percent conversion and high-molecular-weight polymers [114]. Step polymerization distinguishes between polyaddition and polycondensation, accompanied by releasing low-molecular products (e.g., water).

In comparison, chain polymerization is initiated by a reactive species $\mathrm{R}^{\bullet}$, free radical or ion, produced from a compound termed an initiator I [114]. The high-molecular-weight polymer is formed immediately. Chain polymerization can be divided into radical and ionic depending on the reactive center. Radical chain polymerization comprises a sequence of three steps:

1. *Initiation* - the production of a pair of free radicals from the initiator

$$\mathrm{I} \xrightarrow{\mathrm{k}_d} 2\,\mathrm{R}^{\bullet}, \tag{1.11}$$

   and the addition of radical to the first monomer molecule M to form chain-initiating species

$$\mathrm{R}^{\bullet} + \mathrm{M} \xrightarrow{\mathrm{k}_i} \mathrm{M}_1^{\bullet}, \tag{1.12}$$

   where k_d and k_i represent the catalyst dissociation and initiation rate constants, respectively.
2. *Propagation* - the growth of chain-initiating species by the successive additions of large numbers of monomers, generally

$$\mathrm{M}_{\mathrm{n}}^{\bullet} + \mathrm{M} \xrightarrow{\mathrm{k}_p} \mathrm{M}_{\mathrm{n+1}}^{\bullet}, \tag{1.13}$$

   where k_p is the rate constant of propagation. Each reaction creates a new radical enriched by one monomer unit.
3. *Termination* - can occur either by recombination creating a dead end

$$\mathrm{M}_{\mathrm{n}}^{\bullet} + \mathrm{M}_{\mathrm{n}}^{\bullet} \xrightarrow{\mathrm{k_{tc}}} \mathrm{P}_{\mathrm{n+m}}, \tag{1.14}$$

   or by disproportionate

$$\mathrm{M}_{\mathrm{n}}^{\bullet} + \mathrm{M}_{\mathrm{n}}^{\bullet} \xrightarrow{\mathrm{k_{td}}} \mathrm{P}_{\mathrm{n}} + \mathrm{P}^{\mathrm{n}}, \tag{1.15}$$

   where k_{tc} and k_{td} are the rate constants of depicted processes.

It often happens that the growing polymer terminates prematurely via the transfer of atoms from a present compound in the system. This specific chain-braking reaction is called the *chain transfer* and may be depicted as

$$\mathrm{M_n^{\bullet} + XA \xrightarrow{k_{tr}} M}_n\mathrm{-X + A^{\bullet}}, \tag{1.16}$$

where XA may be monomer, initiator, solvent, or other substance and X is the atom or species transferred [114].

1.5.1 Plasma polymerization

Tibbitt, Bell, and Shen in 1977 pioneered a kinetics model of plasma polymerization of thin films. A proposed mechanism for the plasma polymerization of hydrocarbon monomers consists of six possible steps [115]:

Initiation	$\mathrm{e + M \longrightarrow 2\,R^{\bullet} + e},$
Radical adsorption	$\mathrm{S + R^{\bullet} \longrightarrow R_s^{\bullet}},$
Homogeneous propagation	$\mathrm{R_n^{\bullet} + M \longrightarrow R_{n+1}^{\bullet}},$
Heterogeneous propagation	$\mathrm{R_{sn}^{\bullet} + M \longrightarrow R_{s(n+1)}^{\bullet}},$
Termination	$\mathrm{R_m^{\bullet} + R_n^{\bullet} \longrightarrow P_{m+n}}$ or
	$\mathrm{R_m^{\bullet} + R_{sn}^{\bullet} \longrightarrow P_{s(m+n)}^{\bullet}},$
Reinitation	$\mathrm{e + P_{n+m} \longrightarrow R_m^{\bullet} + R_n^{\bullet}}$ or
	$\mathrm{P}_s \xrightarrow{\mathrm{e}, h\nu, \mathrm{I}^+} \mathrm{R_{sm}^{\bullet} + R_{sn}^{\bullet}},$

where e, M, R, and P refer to electron, monomer, radical, and polymer fragment, indices s and g designate substrate and gas, respectively. The plasma polymerization process involves reactions both between plasma species and surface species. After less than a decade, Yasuda proposes a bi-cyclic rapid-step polymerization as the polymer growth mechanism. In particular, he distinguishes the contribution of mono and bi-radicals to the overall polymer formation [92].

1.5.2 Chain fragmentation and degradation

One of the main characteristics distinguishing plasma polymers from conventional ones is the process of chain fragmentation (i.e., the loss of functional groups, ring opening) due to high energy input [116]. The breakage of chemical bonds requires dissociation energy which is at least as high as the bond energy of atoms. The dissociation energy also depends on the atom's chemical environment, details of which can be found elsewhere [117].

During the process of fragmentation, oligomeric units of different lengths are formed. Re-polymerization of oligomers generally leads to highly branched and crosslinked structures. Hence, plasma polymers are considered to be highly complex, three-dimensional networks [83].

The degree of crosslinking strongly depends on the structure of polymerizing molecules (e.g., linear chains vs. aromatic rings), and the crosslinked polymeric matrix is always penetrated by oligomers or even monomers. The relative percentage of low-molecular-weight oligomers embedded in the crosslinked skeleton highly depends on the power input [83].

In addition, a considerable amount of free radicals is often trapped within the network, making plasma polymers reactive after plasma polymerization [116]. Hence, when the plasma polymer is exposed to air, free radicals react with oxygen and water vapor, causing aging processes [116]. Different attempts have been proposed to stabilize the outcome structure (e.g., pulsed plasma polymerization, copolymerization, thermal annealing, etc.). Plasma polymers are thus of disordered structure, randomly branched, and post-reactive, making the plasma polymerization theory rather complicated.

The degradation and stability of plasma polymers have been largely studied with thin film deposition in the gas phase. Despite its recognition, the literature on plasma polymerization in/in contact with liquid is disproportionately thin. Understanding the physical interactions between atmospheric-pressure plasma and liquid state is crucial for film-forming biopolymer solutions and will be one of the main objectives of this study.

1.6 Advances in plasma modification of biopolymers

Amongst the variety of surface modification techniques, atmospheric-pressure plasma treatment represents a flexible, chemically devoid, eco-friendly process enabling to tailor materials' mechanical, structural, and barrier properties, especially in the case of biomaterials, where surface development promises direct application in food packaging.

Non-thermal plasma processing was found to be effective mainly in preventing bacterial attachment [118]. Cold plasma technology can be applied directly to plastic packaging, with significant surface decontamination and tuned physical properties (e.g., an increase of surface energy and surface roughness, improved oxygen barrier function) and food, without losing nutritional content [119].

In comparison with plastic packages, biopolymer-based packaging materials are known to exhibit poorer mechanical and adhesion properties. Exposure of biopolymer, either in the liquid or solid state, to non-thermal plasma may alter the structure of the biopolymer.

Chitosan is soluble in dilute acidic solutions, being an undesirable effect not only in packaging but especially in agrotechnology, where the use of water-soluble fertilizers is inevitable. Chitosan was already shown to undergo structural modification via solution plasma processing. As aforementioned, exposure of biopolymer to non-thermal plasma leads to the breakage of chemical bonds and chain degradation. Consequently, lowering the molecular weight should improve the biopolymer's solubility.

Tantiplapol et al. studied the effects of solution plasma on β-chitosan's degradation rate and properties [120]. The solution plasma was operated in ambient air with a pulsed power supply. The experimental results showed a reduction in the molecular weight of plasma-treated chitosan with increasing treatment time. Furthermore, they found that the degradation rate was affected by the types of electrodes and the applied pulse frequency. The degradation process left chitosan's chemical structure unaffected. Another study focused on *in-situ* treatment of polypropylene foils immersed in chitosan solution via DC atmospheric glow discharge with a liquid cathode [106]. The treatment led to the depolymerization of chitosan and polypropylene with the formation of chitooligosaccharides.

Despite the many benefits of sodium alginate (i.e., biocompatibility, high solubility, and ease of gelation), the brittleness of alginate-based films and coatings is one of the biggest obstacles to overcome. The mechanical properties of alginate are often improved by the addition of plasticizers (namely glycerol and sorbitol) [121]. The cross-linking mechanism of plasma polymerization might be another approach to improving alginate's flexibility.

Only a limited number of studies have been assessed on the solution plasma processing of sodium alginate, and if so, they were accessed to observe the biopolymer's depolymerization. In particular one [122], the depolymerization of the alginate via SPP was affected by two important factors: (1) the number of reactive species generated during the process and (2) the degree of chain entanglement of the polymers. However, many studies have improved the functionalization of alginate films with various additives. *Santos et al.* developed sodium alginate active films incorporated with purple onion peel extract (POPE) [123]. The pres-

ence of high phenolic compounds in POPE induced higher antioxidant activity of alginate films. Moreover, most extract films showed less solubility in water, justified by the interactions of the anthocyanidin cations with the alginate network, providing the cross-linking of the material. In another work, thyme oil was incorporated into sodium alginate-based coatings to investigate the mechanical, antioxidant, and preservation properties of fresh-cut apples [124]. The addition of thymol resulted in increased tensile strength and elongation at break, probably due to the formation of intermolecular hydrogen bonds between thymol and alginate chains. The antioxidant and antibacterial properties of thymol were of further benefit for the packaging application.

2. Materials and methods

2.1 Materials

β-chitosan (molecular weight 197 kDa, DD = 82%) was obtained by the deacetylation of chitin in Bioprogess Ltd, Russia. Low and medium-viscosity sodium alginate from brown algae and almond essential oil (bitter) were purchased from Sigma-Aldrich.

2.2 Solution preparation

β-chitosan acetic acid solutions were prepared by dissolving 4 g of biopolymer in 400 mL 2% acetic acid solution (pH = 2.4) in water under 20 min constant stirring at 50 °C to obtain a 1% (w/v) chitosan solution.

Low and medium-viscosity sodium alginate powder was dissolved in distilled water to obtain 0.2, 0.5, and 0.9% w/v aqueous solutions inspired by previous studies [122]. For the preparation of film-forming solution incorporated with EO, 1.0, and 10 mg mL^{-1} of almond oil bitter was added to alginate in solution ([82]).

2.3 Solution plasma system with DC discharge for chitosan processing

Fig 1. shows the experimental setup used for plasma processing β-chitosan.

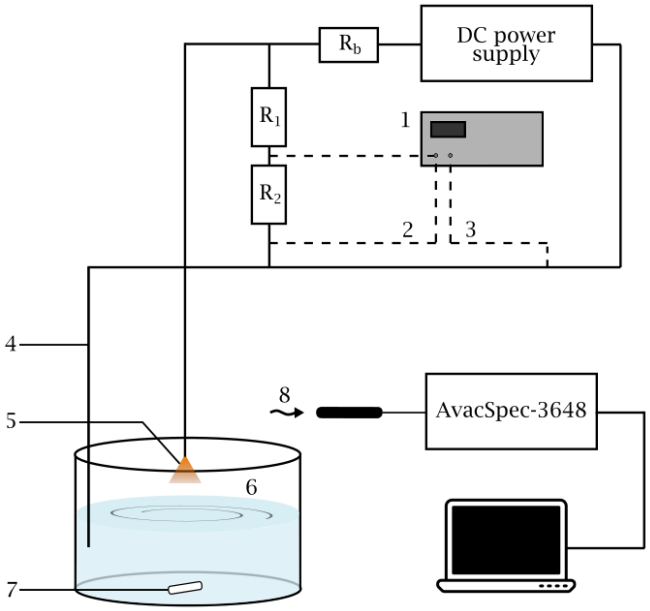

Figure 2.1: Set-up of DC glow discharge in ambient air for β-chitosan solution plasma processing: 1) oscilloscope, 2) voltage measurement, 3) current measurement, 4) anode, 5) glow discharge, 6) cathode, 7) magnetic stirrer, 8) *in-situ* OES.

A DC power supply ignited a glow discharge between a graphite rod electrode, the anode, and the surface of the chitosan solution, the cathode. The distance between the anode and cathode was 4 mm. The glow discharge was operated in ambient air at 48 W. Chitosan was treated in solution for 20 min.

2.4 Atmospheric pressure plasma jet for alginate processing

The experimental setup adapted by[101] is presented in fig. 2.2. The RF power supply (Dressler Ceasar, 13.56 MHz) was used for igniting the non-thermal atmospheric plasma used for the treatment of alginate solutions.

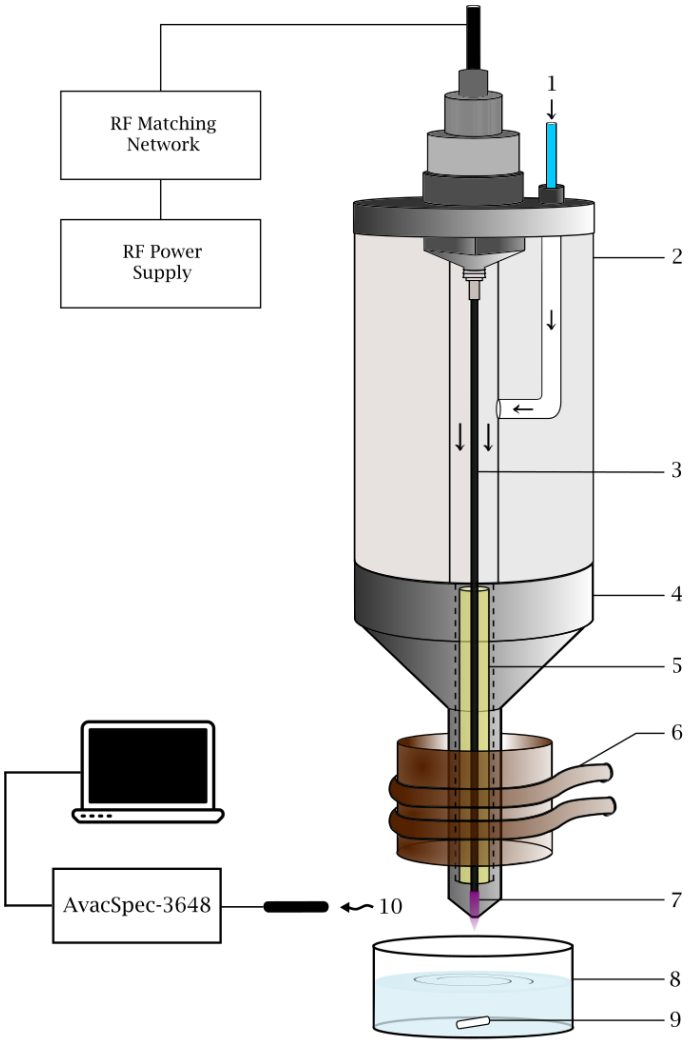

Figure 2.2: Set-up of APPJ for alginate solution processing: 1) working gas inlet, 2) PTFE cylinder, 3) cathode, 4) anode, 5) ceramic insulator, 6) water cooling system, 7) afterglow, 8) plasma-treated solution surface, 9) magnetic stirrer, 10) *in-situ* OES.

The treatment process was produced with Ar ($2\,\mathrm{L\,min^{-1}}$) or Ar/air mixture ($0.049/1.5\,\mathrm{L\,min^{-1}}$) at 35 W. The flow was regulated using calibrated glass tube

flow meters. The solution treatment was performed for 4, 8, 16, 32, and 48 min. The distance between the APPJ afterglow and solution surface was kept constant at 9 mm for all treatments.

2.5 Preparation of water-soluble and insoluble chitosan fractions

The fractionation of the plasma-treated chitosan solution was conducted to obtain the water-insoluble and water-soluble fractions [125]. The plasma-treated solution was neutralized by NaOH up to pH 7.5. The resulting first precipitate was removed by centrifugation at 6000 rpm for 15 min from which the water-insoluble fraction was obtained.

An equal volume of acetone was added to the supernatant and mixed. The second precipitate (water-soluble fraction) was centrifuged under the same conditions. Both the first and second residues were dried in an oven at 55 °C for 48 h.

2.6 Preparation of alginate films

After APPJ treatment in liquid-state, sodium alginate films were prepared via the casting technique on glass Petri dishes (Ø = 51 mm). Casting volume was chosen 3 mL to obtain 10 - 30 µm thick foils. Samples were naturally dried in the atmosphere for 24 h hours without controlling the evaporation rate. After solvent evaporation, the foils were gently peeled from the glass surface and stored in ambient air for further characterization. Films incorporated with EO were produced by the same technique.

2.7 Characterization methods

2.7.1 Optical emission spectroscopy

Optical Emission Spectroscopy (OES) provides elemental analysis due to the emission of light by matter. Basically, the emission spectra are the energy spectra of photons emitted during the relaxation of the excited electronic state to the ground state [126]

$$M^* \rightarrow M + h\nu, \tag{2.1}$$

where $h\nu$ is the photon energy. Species immersed in plasma may emit several types of radiation when interacting with light. *Line radiation* occurs when a bound electron undergoes a transition from an upper energy level (II) to a lower energy level (I). The frequency of the emitted radiation $\nu_{II \rightarrow I}$ is simply given by the energy difference between the two states [127]

$$\nu_{II \rightarrow I} = \frac{E_{II} - E_I}{h}. \tag{2.2}$$

This transition is spontaneous, and the emission is proportional to the density of the charged species in the excited state n_{II} [127]. The fundamental spectroscopic equation for the line emission reveals that the emission coefficient $\varepsilon_{II\to I}$, defined as the amount of emitted energy, is proportional to the population densities of the excited states n_{II} [127]

$$\varepsilon_{II\to I} = \frac{h\nu_{II\to I}}{4\pi} A_{II\to I} n_{II} \mathcal{L}(\nu), \tag{2.3}$$

where $A_{II\to I}$ is the Einstein coefficient of spontaneous emission, and $\mathcal{L}(\nu)$ is the profile function, describing the broadened shape of spectral lines. With each transition, a photon with a unique frequency for each atom or molecule is emitted. Thus, the spectral lines may thus provide information about the plasma composition.

Besides line radiation, two continuous radiations may also occur. The *recombination radiation* happens when electrons recombine with ions. *Bremsstrahlung* (free-free radiation) is emitted when the electrons experience deflection (acceleration or retardation) in the electric field of the ions [127].

In the case of molecules and molecular ions, electronic states α are split into vibrational levels ν, and these again into rotational ones J. Emission between rotational levels is typically in the microwave region, between vibrational levels in the infrared region, and the spectrum lines in the UV-vis region correspond essentially to electronic transitions [127].

In this study, OES was used for the elemental analysis of the atmospheric pressure low-temperature plasma jet. Time-averaged emission spectra were recorded by Avantes spectrometer (AvaSpec 3648) in the range of $300 - 850\,\mathrm{nm}$.

2.7.2 Capillary viscosimetry

Capillary viscosimetry, or dilute solution viscosimetry, provides a quantitative measurement of the increase in viscosity and allows the determination of the intrinsic viscosity of dilute polymer solutions at a given temperature. It is a simple, fast, and inexpensive method, applicable over the complete range of accessible molecular weights.

The intrinsic viscosity is measured experimentally by a capillary-based method using an Ubbelohde viscometer. An accurate volume of the solvent (15-17 mL) is introduced through a filling tube into the reservoir and drawn to the set volume above the upper mark. As the solution flows down, the flow time between the upper and lower mark is measured. The experiment is then repeated with different polymer concentrations.

The mathematical background of this method stands on a set of simple equations

$$\eta_{sp} \approx \frac{(t - t_0)}{t_0}, \tag{2.4}$$

$$\eta_{red} \approx \frac{(t - t_0)}{ct_0}, \tag{2.5}$$

$$\eta_{inh} \approx \frac{\ln \eta_{red}}{c}, \tag{2.6}$$

$$\eta_{red} = k'[\eta]^2 c + [\eta], \tag{2.7}$$

$$\eta_{inh} = k''[\eta]^2 c + [\eta]. \tag{2.8}$$

From the intrinsic viscosity $[\eta]$, the average molecular weight can be calculated using Mark-Houwink equation [128]

$$[\eta] = KM^a, \tag{2.9}$$

where K and a are constants specific to each polymer-solvent combination.

DSV of low and medium-viscosity plasma-treated sodium alginate solutions was measured in the Ubbelohde tube viscometer (with a capillary 0.56 mm in diameter) equipped with an electronic viscosity measuring unit and automatic flow-time meter (ViscoClock, SI Analytics). 15 mL of distilled water was introduced as the solvent, then successively 0.5 mL of treated 0.2% (w/v) solution was added up to 17 mL. A viscometer was placed in the thermostat to ensure stable temperature $(20.0 \pm 0.2)^\circ$C during all measurements. Each measurement was repeated thrice with 15 min stabilization time between concentration exchanges. The specific viscosity of these solutions was measured, and the intrinsic viscosity was determined by performing the extrapolation. The $\mathrm{K} = 7.3 \times 10^{-3}\,\mathrm{mL\,mol\,g^{-2}}$ and a = 0.92 values for sodium alginate in water solutions were taken from [129].

2.7.3 Gel permeation chromatography

Gel Permeation Chromatography (GPC), or also Size-Exclusion Chromatography (SEC), is a frequently applied technique used for: [130]

1. preparing molecular fractions for characterization or further use,
2. desalting or buffer exchange,
3. estimating molar mass using calibration standards or an absolute method (e.g. light scattering),
4. estimating molecular association constants.

As the name indicates, its principle is sorting molecules according to their size in solution. Once a polymer is dissolved, long chains of monomers coil up in tiny spheres with the size dependent on the molecular weight. Due to chain polydispersity, neither natural nor synthetic macromolecules comprise equally sized segments. This phenomenon plays a key role in the size separation mechanism.

The polymer solution is injected in a small volume onto the column of porous structure and carried by solvent through the column (mobile phase) [130]. As they flow through the column, polymer coils larger than the given pore's size are carried right to the detector, whereas the smaller ones enter the pores (stationary

phase), diffuse back, and come delayed. Thus, the coils migrate through the column with different velocities.

At the end of the experiment, different sizes of polymer coils are separated, and their concentration is detected as a function of the retention volume V_R [130]. The larger the size of the eluting solute molecule, the smaller V_R. The measurement results in a chromatogram where separate or broad peaks appear, depending on the polymer molar mass distributions. To extract this information from the raw data, a M-V_R calibration curve needs to be established [130].

The molar mass distribution of the β-chitosan water-soluble fraction was studied using an Agilent 1260 Infinity GPC/SEC setup equipped with a differential refractometric detector. Two PLGEL columns of porosities 100 and 10 000 L/5 µL were used with the THF flow rate 0.8 mL min^{-1} at 30 °C.

2.7.4 Nuclear magnetic resonance spectroscopy

Nuclear Magnetic Resonance (NMR) spectroscopy is a powerful technique providing information about the structure and dynamics of molecules. The basic physical principle behind the NMR lies in the magnetic properties of certain nuclei. All nuclei carry a charge, and in some cases, this charge "spins" and creates a magnetic dipole moment μ. Nuclei with the quantum spin number $I = \frac{1}{2}$ can be readily measured [131]. Of these, isotopes ^{1}H and ^{13}C are most widely used for obtaining the NMR spectra.

In the presence of an external magnetic field, the rise of energy levels occurs. The energy difference between the two spin states is dependent on the external magnetic field B_0 as [131]

$$\Delta E = \hbar \gamma B_0, \tag{2.10}$$

where γ is the gyromagnetic ratio and $\hbar$ is the reduced Plank's constant. As we measure a compound with many nuclei, the observed NMR signal comes from the contribution of all magnetic moments μ_i defined by the magnetization vector $\vec{M}$. Parallel to the direction of the applied magnetic field B_0 [132], if $\vec{M}$ is slightly tilted away, it exhibits Larmor precession with a characteristic frequency ω_0 given by [132]

$$\omega_0 = -\gamma B_0. \tag{2.11}$$

The precession of $\vec{M}$ is what we actually detect in the NMR experiment [132]. To ensure this particular motion, a radiofrequency (RF) pulse is applied to the compound with a frequency ω_1. If the frequency matches the precessional frequency ω_0, the resonance condition is satisfied, proton absorbs energy and raises to higher energy (spin) state [131].

According to eq. 2.11, only a single proton peak should be expected from the interaction of RF pulse and B_0. In reality, each proton is shielded with its electron cloud, the density of which varies regarding its chemical environment [131]. When measuring molecules, a correction to slightly different frequencies is processed by *chemical shift* δ, relative to a standard reference compound [131]. Due to *J-coupling*, a spin-spin interaction of chemically nonidentical nuclei, peak splitting is observed in the NMR spectra giving information about the fine molecule

structure. Furthermore, the integral area of the peak intensities may provide information about the nuclei concentration present in the compound.

In this study, ^{1}H NMR spectra of dissolved untreated and plasma-treated chitosan and sodium alginate were recorded at 500.17 MHz by an Avance III (Bruker) spectrometer equipped with a 5 mm TBI z-GRD probe. The spectra were referenced to external standards of hexamethyldisiloxane (HMDSO).

Two β-chitosan NMR measurements were done, in D_2O and DCl/D_2O solution. For the first, 6.4 mg of untreated chitosan, 5.9 mg of water-soluble fraction, and 5.4 mg of the water-insoluble fraction were dissolved in 0.6 mL D_2O. Samples were heated at 70 °C under 80-minute constant stirring. For the latter, 50 µL DCl (34%) was added to 0.6 mL D_2O chitosan solutions. The samples were kept at 50 °C for 1 h under constant stirring. The assignment of the spectral signals was performed according to [133], [134], and [106].

Sodium alginate (0.9% w/v) was dissolved in D_2O. NMR measurements were performed for solutions treated in Ar and Ar/air plasma for 32 min. These samples were directly measured at 330 K.

2.7.5 Ultraviolet-visible spectrophotometry

Ultraviolet-visible (UV-vis) spectrophotometry is a non-destructive quantitative and qualitative method used to obtain light absorbance or transmission spectra of a compound in a solution or solid-state. The light intensity loss during the propagation through a medium is defined by Lambert-Beer law [135]

$$A = \varepsilon c l, \tag{2.12}$$

where ε is an molar absorption coefficient, c molar concentration, and l optical length. When an atom or molecule absorbs energy, an excitation to a higher electronic energy state occurs, associated with vibrational and rotational levels [135]. The absorption usually involves the excitation of bonding electrons. Therefore, the wavelengths of absorption bands can be correlated with the types of bonds in the studied sample [135].

In organic compounds, the absorption of UV and visible radiation is restricted to a certain number of functional groups called *chromophores*, such as carbonyl, carboxyl, amido, azo, or nitro groups, that contain valence electrons of low excitation energy. On the other hand, *auxochromes* are covalently saturated groups attached to chromophores that do not absorb in the UV-vis region but affect the position and the intensity of the absorption band. Common examples are halogens, or $-NH_2$ and $-OH$ groups. Auxochromic substituents have at least one pair of n electrons capable of interacting with the π electrons in the chromophores' structure [135]. This interaction stabilizes the excited $\pi*$ state, thereby lowering its energy and increasing the wavelength of the corresponding band. Shift to longer wavelengths is called a *bathochromic* or *red shift*. A shift to shorter wavelengths is called a *hypsochromic*, or *blue shift*, caused by the removal of conjugation or change in the solvent's polarity [135].

Due to various effects occurring at the interfaces of the cell (such as beam reflection at the interfaces, scattering, or absorption by the container walls), the

beam transmitted by the analyte solution is often compared with the power P of the beam transmitted by the same cell containing only solvent [135]

$$A = \log \frac{P_{\text{solution}}}{P_{\text{solvent}}} \approx \log \frac{P_0}{P}. \tag{2.13}$$

For this study, UV–Vis spectrophotometer (Hitachi U-2900) was used in the range 190–700 nm (scan speed 400 nm min^{-1}, sampling interval 1 nm). Absorbance spectra were measured for low and medium-viscosity alginate solutions (0.2, 0.5, 0.9 % w/v) treated in pure Ar and Ar/air mixture for $4, 8, 16, 32$, and 48 min. Analyte solution was poured to (10 mm) quartz cuvette. Distilled water was used as the reference solvent.

2.7.6 Fourier-transform infrared spectroscopy

Fourier Transform Infrared (FTIR) spectroscopy is a fast, non-destructive analytical technique that almost entirely replaced dispersion IR spectrometers. Unlike the latter, FTIR spectrometers measure radiation from all wavelengths simultaneously and not successively [136], making the measurements much faster. Radiation containing all IR wavelengths enters the Michelson interferometer and splits into two beams. As the distance between two path lengths varies, the beams interfere and create an interferogram. By applying a mathematical operation (Fourier transform) to raw data, a frequency spectrum can be obtained.

And yet, despite the differences, the principle of infrared or vibrational spectroscopy is the same for all the techniques. The inelastic collisions between electromagnetic radiation and molecules may produce characteristic vibrations of varying modes (dependent on the nature of the bond) with a unique vibrational frequency [137]. IR spectrum depicts the transmittance T dependence on the wavenumber ν, defined as the inverse value of wavelength λ, with characteristic peak frequencies assigned to unique functional group stretch. Thus, a precise chemical analysis of the studied compound can be determined.

As a complementary technique, Attenuated Total Reflection (ATR) FTIR is used to qualify the samples directly in either a solid or liquid state, without additional preparation.

The FTIR analysis was performed by Vertex 80 V (Bruker) spectrometer. Measurements in Attenuated Total Reflection (Nicolet 6700, Thermo Scientific) were done using a ZnSe crystal.

2.7.7 Nanoindentation

Nanoindentation is a non-destructive technique providing information about various physical parameters (elastic or shear modulus, hardness, strain-hardening, cracking, phase transformations, etc. [138]). Measurement in dynamic mode enables to study of material transitions and viscoelastic properties as a function of temperature, frequency, or time.

The basic principle of nanoindentation testing stands on a continuous measurement of the penetration depth beneath the specimen surface as the load is

applied to the indenter [138]. With the known geometry of the indenter (spherical, conical, Vickers, or Berkovich), the size of the area of contact A can be determined [138]. In the frequency sweep mode, a Berkovich tip is brought in contact with a sample at a fixed load, then the dynamic load is applied at a fixed amplitude and the frequency is varied in progressive steps- Mechanical properties of viscoelastic materials are obtained in terms of complex modulus G*, storage modulus G', and loss modulus G" [138]

$$\mathrm{G}^* = \mathrm{G}' + i\mathrm{G}'' \tag{2.14}$$

$$\tan\delta = \frac{\mathrm{G}''}{\mathrm{G}'}. \tag{2.15}$$

Nano-DMA was performed on sodium alginate films drop cast on glass (1.5×1.5 cm). Plasma-processed solutions (0.9% w/v) were treated in Ar and Ar/air mixture for 48 min. A series of indentations were made at a fixed load of 500 µN, the amplitude of dynamic load 1 µN in the frequency range of 0.1 - 300 Hz. On each sample, data were acquired at three different spots and then the values were averaged. The data obtained at the lowest frequency of 0.1 Hz were very noisy and not always reliable.

2.7.8 Antibacterial activity

Metabolic activity measurements were applied to evaluate the antibacterial effect of plasma-treated alginate films incorporated with different concentrations of almond EO. Initially, 10 µL of food-borne Gram-negative bacteria Escherichia coli (strain Seattle 1946; ATCC 25922) was diluted in 30 mL CASO Agar culture medium (Carl Roth®) to obtain a concentration of 50 000 CFU/mL. The bacteria were incubated at 37 °C and agitated with a frequency of 180 rpm overnight.

The foils were initially sterilized with UV radiation for 30 min. The triplicates of foils (1.5×1.5 cm) were placed into a 12-well plate. Then 57 µL of the bacterial suspension was added, covered by a micro glass, and incubated at 37 °C. A control bacterial suspension was incubated under the same conditions without adding the film.

After 24 h of the incubation period, 100 µL of bacteria suspension diluted with 500 mL of CASO medium and AlamarBlue^{TM} reagent (Invitrogen) of 10:1 (v/v) ratio was transferred into a 96-well plate and incubated for 5 min. The bacteria concentration was measured using a fluorescence spectroscope Infinite M200 (Tecan) with excitation wavelength 550 nm and emission wavelength 590 nm, where the intensity of the produced fluorescent signal is quantitatively proportional to the number of metabolically active bacteria.

2.7.9 Preparation of alginate coatings of tables grapes

Fresh table grapes (Sweet Joy®; IFG Seventeen, California) were purchased from a wholesale distributor in the Czech Republic and processed 2 h after the purchase. Fruits were selected according to shape, color, size, and firmness, with no signs

of mechanical injury or fungal infection. For the experiment, 1 and 10 mg mL^{-1} of almond oil were selected in coherence with earlier results ([139], [124]). Low-viscosity alginate (0.9% w/v) was used as the coating solution treated by Ar or Ar/air for 32 min. For the edible coatings application, a spraying technique was used with a standard spray nozzle detached from washed and sterilized spray system.

Grape clusters were divided into five groups of 10 single berries detached from branches. They were carefully washed in distilled water for 2 min, dried in a paper towel, and placed in Petri dishes ($\varnothing = 14.4$ cm) to proceed a 10 min UV treatment (15 W). Alginate coating was applied at ambient temperature on the whole surface of one grape at a time from both sides from a 20 cm distance; ~ 10 µL of sprayed volume was homogeneously applied on both sides of the grape. Grapes without spraying were used as a control group. Both control and coated grapes were then stored in a cleaner box at 24 °C and 44% RH for 18 days. No additional chemicals were used to enhance the polymer crosslinking.

The weight loss (WL) was calculated by using the following formula and recorded with an accuracy of 0.01 g

$$\text{WL } (\%) = \frac{m_0 - m}{m_0} \times 100\%, \tag{2.16}$$

where m is the current fruit weight and m_0 is the initial fruit weight. The grapes were weighted every three or four days (3, 6, 10, 14, and 18).

3. Results and discussion

3.1 Plasma processing of sodium alginate for the production of functional materials

Sodium alginate demonstrates strong potential to be employed for the production of biocompatible and biodegradable foils for different applications, such as medicine or food storage. The main drawback limiting alginate‘s use lies in poor mechanical properties that should be typically improved by adding chemical plasticizers. In this chapter, the APPJ will be described as a potential instrument for plasma polymerization of sodium alginate to modify the functional properties of resulting films and also produce novel composite materials with advanced properties.

Two approaches using Ar and Ar/air mixture as working gas will be compared. First, the characterization of discharge will be described. Further, the demonstration of plasma influence on alginate in the solution will be demonstrated. The solution analysis proceeds to the detailed characterization of foils based on plasma-processed alginate solutions. Finally, the application of APPJ for the preparation of novel composite materials using a combination of sodium alginate/essential oil will be demonstrated.

3.1.1 Plasma diagnostics of APPJ

First, the plasma diagnostic of APPJ was carried out by OES. Optical emission spectra were acquired for pure Ar and Ar/air mixture to analyze the differences in the chemical composition of plasma. Measurements were performed at the discharge power of 35 W, which was further utilized in most of the experiments.

Fig. 3.1 shows the emission spectra, and the most intensive emission lines are listed in the tab. 3.1. Signals of many species were observed in pure Ar plasma. The most intense lines can be observed in the range of 690 – 850 nm corresponding to the series of excited states of atomic Ar. The Ar I line situated at 763.7 nm is the most intensive one. Two atomic oxygen (O I) spectral lines can be observed at 777.2 nm and 844.8 nm resulting from O_2 molecules dissociation. Moreover, hydroxyl radicals ($OH^{\bullet}$, transition $A^2\Sigma^+$–$X^2\Pi$) and the second positive system of nitrogen (N_2 SPS) signals can be detected in the region 300 – 450 nm. The same signals have been detected earlier in spectra of Ar plasma acquired for similar construction of APPJ [140].

Consistent with the study of *Sarani et al.*, the transition of $OH^{\bullet}$ rotational band at 308 nm is responsible for the production of significant UV radiation [141]. Weak emission signals of the SPS of N_2 detected in the range 310 – 440 nm most likely originated from the diffusion of N_2 molecules from the ambient atmosphere into the plasma zone.

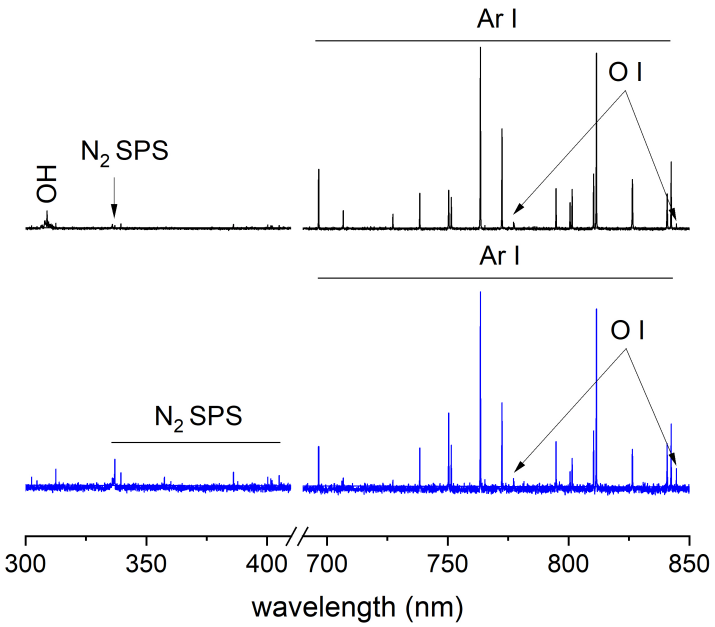

Figure 3.1: OES spectra of APPJ afterglow recorded in (●) Ar and (●) Ar/air.

species	λ (nm)	λ^a_{ref} (nm)
OH	308	308.4900
N_2 SPS	336.9	336.7340
O I	777.2	777.1940
O I	844.8	844.6760
Ar I	696.4	696.5431
Ar I	751.5	751.4652
Ar I	763.7	763.5106
Ar I	772.6	772.3761
Ar I	811.8	811.5311
Ar I	826.3	826.4522
Ar I	842.6	842.4648

Table 3.1: Most intensive emission lines of plasma afterglow species in Ar and Ar/air mixture.

[a]Detected lines are compared to observed wavelengths from NIST Atomic Spectra Database Lines Data.

The addition of air to Ar leads to an increase in the intensity of signals corresponding to atomic O and the second positive system of N_2. Moreover, the band at 308 nm corresponding to $OH^\bullet$ was substantially suppressed. According to [142], this phenomenon might be correlated with a decrease in electron temperature T_e at the higher content of molecular species in the working gas mixture. The addition of N_2, O_2, and H_2O to noble gas discharge results in worse energy transfer efficiency between electrons and other species, causing a T_e drop.

Another possible reason for the hydroxyl signal vanishing lies in their more efficient recombination due to the appearance of additional pathways. According to the model proposed by authors of [143], the $OH^\bullet$ can recombine in the reactions

with $O_2^{\bullet-}$, $NO^{\bullet}$, $NO_2^{\bullet}$ and O_3. Especially the ozone formation in the Ar/air mixture was confirmed by the appearance of a characteristic smell. Another interesting effect of air addition was manifested in the transformation of the jet's color and shape. After the air addition, the color changed from purple to milk-white and the length of the afterglow substantially increased.

3.1.2 Characterization of alginate solutions

Atmospheric pressure plasma is a well-known tool for the modification of polymeric materials. One of the main advantages of APPJ is the opportunity to process solids as well as liquids. In this work, the APPJ was applied to treat sodium alginate solutions used further for casting foils.

I. Determination of molar mass

First, the result of plasma action was characterized by means of capillary viscosimetry because the polymer degradation assumes to be the main effect. The average molar mass M of sodium alginate was determined from the measured intrinsic viscosity $[\eta]$ of alginate solutions treated by Ar and Ar/air plasma using the Mark-Houwink equation.

The treatment by APPJ in pure Ar has a surprisingly unique character, see fig. 3.2a. In earlier reported studies, the action of plasma usually resulted in a continuous decrease in the viscosity of biopolymer solutions, a behavior associated with the fragmentation of biopolymer chains and with the formation of oligomers [106].

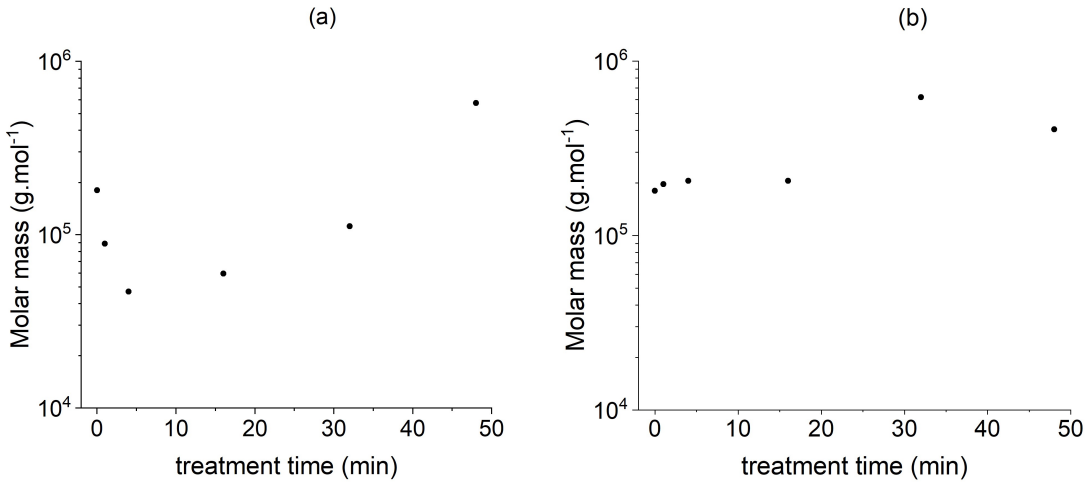

Figure 3.2: The dependence of the molar mass M on the treatment time t of low-viscosity alginate solution (2% w/v) treated in a) pure Ar and b) Ar/air.

However, during the treatment, the solvent continuously evaporates from the treated volume. Especially during high treatment times, water evaporation becomes significant, and the concentration of oligomers in the solution increases. At this point, the re-polymerization occurs, leading to the formation of higher molecular weight species. The M(t) curve acquires a global minimum at 47 kDa for 4 min treatment time, which should correspond to the highest degradation point

of alginate. After 48 min treatment time, the molar mass reaches a maximum of 576 kDa. Compared to the untreated alginate (181 kDa), plasma treatment showed a more than a three-fold increase in polymer molar mass.

Surprisingly, the M(t) dependence of alginate treated in mixed Ar/air plasma does not follow the same behavior. As shown in fig. 3.2b, the molar mass gradually increases with the treatment time, with no local minimum observed. The curve, however, reaches a local maximum after 32 min of plasma treatment with a maximum molar mass 619 kDa. This value again represents a three-fold increase in alginate molar mass.

The immediate increase in molar mass during low treatment times is probably related to the higher rate of solvent evaporation due to solution warming. This suggestion is in perfect coherence with the measurements of temperature-time dependence (tab. 3.3).

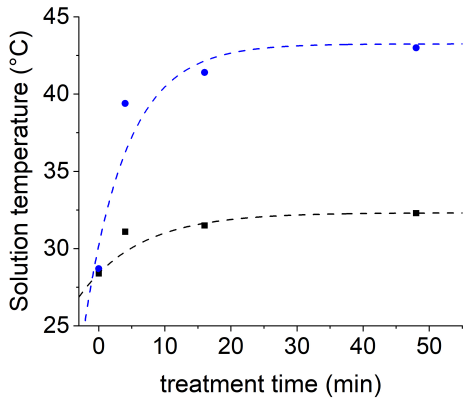

Figure 3.3: Time dependence of the solution (0.9% w/v) temperature measured with a thermoscope during the treatment in (●) Ar and (●) Ar/air.

II. UV-Vis spectra

The concentration dependence of low and medium-viscosity alginate treated via APPJ in Ar and Ar/air is illustrated in fig. 3.4. As expected, both viscosities show very similar absorption properties. Alginate solutions absorb light mainly in the UV region ($100 - 300$ nm) due to the presence of saturated sigma bonds. An intense $\sigma \rightarrow \sigma^*$ electronic transitions around 200 nm belong to C–C and C–H functional groups. After exposing different concentrations of alginate solutions to plasma, a broad continuous absorption band appears at 265 nm. *Nagasawa et al.*, who studied the degradation ability of sodium alginate by gamma rays, assigned the new absorption band at 265 nm to double bonds formed after the scission of main chains and/or hydrogen abstraction reaction by irradiation [144]. A $\pi \rightarrow \pi^*$ electronic transition might be related to forming carbonyl C=O groups. Increasing solution concentration induces higher absorbance of the 265 nm with no band shift observed.

Based on earlier OES results [122], the number of reactive species depends remarkably on the amount of water in the system. For low alginate concentrations, the production of ozone and/or H_2O_2 was reported high enough to reform the single bonds. At higher concentrations, the number of ozone and/or H_2O_2

decreased, and the formation of double bonds predominated. This might explain the intensity increment of the 265 nm band with increasing polymer concentration. Furthermore, this phenomenon is in coherence with the effect of plasma re-polymerization. It is a well-known fact that plasma causes chain fragmentation, and with sufficient energy input, ring opening might occur. Applying plasma to a high-concentrated polymer system leads to the formation of a denser network via the re-polymerization process. Consequently, Ar plasma does not affect the biopolymer's chemical composition but strongly affects the chain structure.

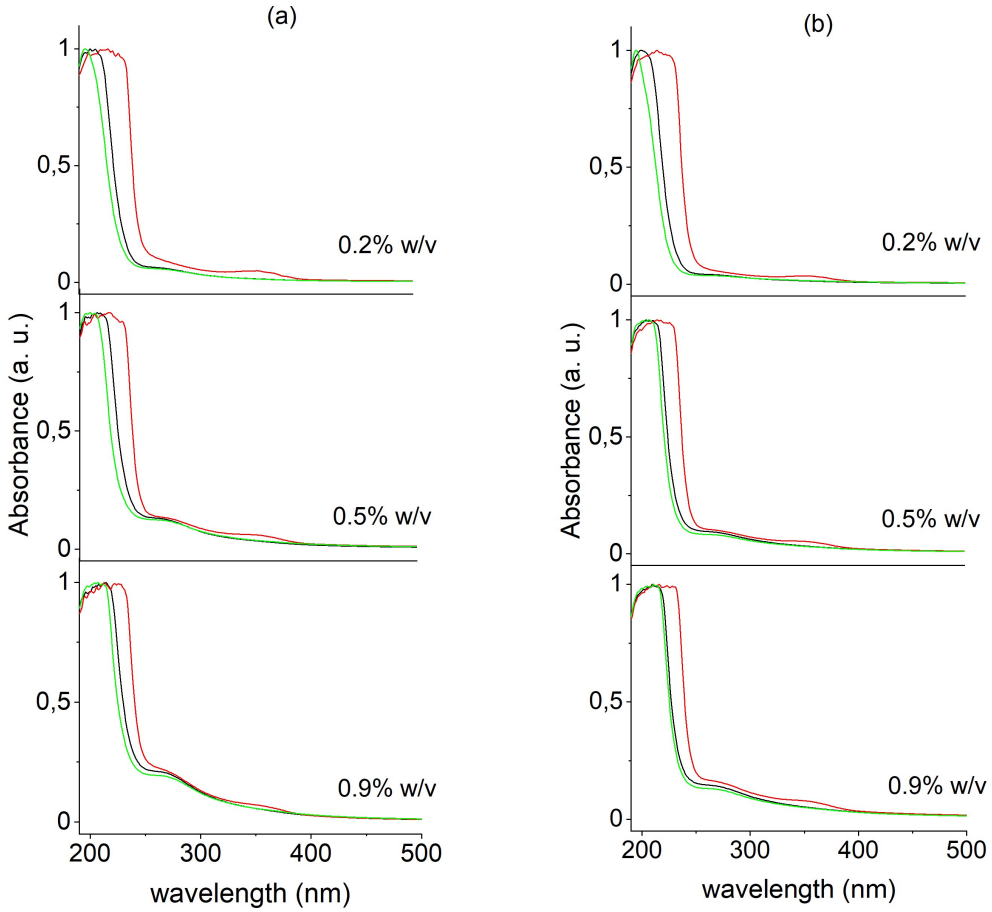

Figure 3.4: UV–Vis spectra of a) low and b) medium-viscosity sodium alginate: (●) control, (●) treated in Ar, and (●) treated in Ar/air for 16 min at 35 W.

Adding air to Ar plasma results in a weak absorption band at 360 nm. APPJ plasma causes the decomposition of not only water and oxygen molecules but also the transformation of nitrogen molecules. According to [145], this band could be assigned to NO_2^- produced in SPP via a possible chemical reaction [146]

$$2\,NO^{\bullet} + O \longrightarrow 2\,NO_2^{\bullet}. \tag{3.1}$$

Low and medium-viscosity alginate solutions follow the same behavior: the integral area of the 360 nm peak acquires maximum for the lowest concentrations, see tab. 3.2. The intensity decrement coincides with the aforementioned statement supported by the study of [122].

Sample		Integral area (a. u.)
low-viscosity	0.2% w/v	0.62
	0.5% w/v	0.26
	0.9% w/v	$\ll 0.1$
medium-viscosity	0.2% w/v	0.44
	0.5% w/v	0.27
	0.9% w/v	0.24

Table 3.2: Integral area fit (G/L) of the 360 nm band for different alginate concentrations treated in Ar/air.

Moreover, the detailed structure of the 360 nm absorption band (fig. 3.5) shows the fine structure of rotational and vibrational levels associated with the excited electronic states of $NO_2^{\bullet}$.

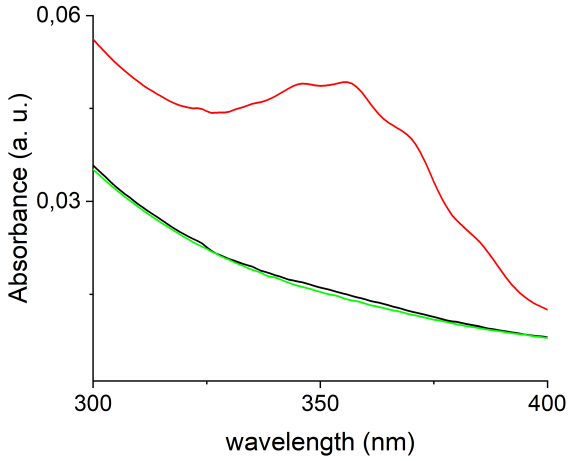

Figure 3.5: Detailed structure of 360 nm absorption band of 0.2% w/v low-viscosity alginate: (●) control, (●) treated in Ar, and (●) treated in Ar/air for 16 min at 35 W.

Fig. 3.6 shows the UV-Vis spectra of low and medium-viscosity alginate (0.9% w/v) treated in Ar and Ar/air during different treatment times. As previously discussed, a band at 265 nm is observed for all samples. Moreover, after 48 min treatment in Ar plasma, a significant increase in the peak intensity occurs for the low-viscosity alginate. This result indicates a higher concentration of the C=O bonds in the alginate structure induced via the action of plasma at high treatment times. A similar phenomenon is observed with the medium-viscosity alginate treated in Ar; however, the intensity of the 265 nm reaches a maximum for the 32 min treatment due to solvent evaporation at high treatment times.

As in the previous case, an absorbance band at 360 nm was observed, assigned to the NO_2^- species with admixing air to Ar plasma. The band's intensity increases with increasing treatment time.

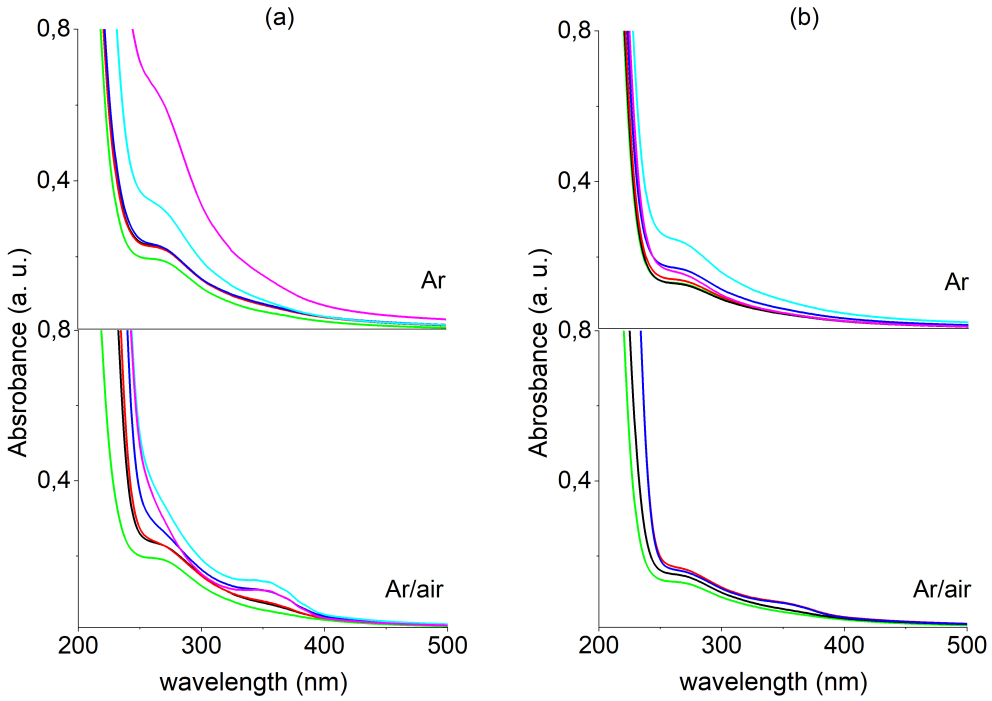

Figure 3.6: UV–Vis spectra of a) low and b) medium viscosity sodium alginate (0.9% w/v) treated in Ar and Ar/air at 35 W during different treatment times: (●) control, (●) 4 min, (●) 8 min, (●) 16 min, (●) 32 min, and (●) 48 min.

The discharge power dependence of low-viscosity alginate after a 16 min APPJ treatment in Ar and Ar/air admixture is shown on fig. 3.7. The purpose of this measurement was to justify our hypothesis on the power independence of the alginate chemical structure. According to the results, no changes occurred even at a high discharge power. For economizing reasons, we continued all the experiments at the possible lowest discharge power 35 W, which could be interesting for future technological approaches.

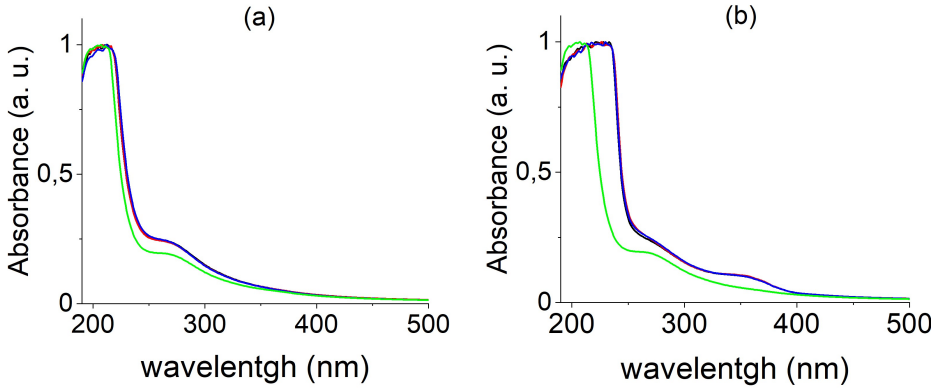

Figure 3.7: UV–Vis spectra of low-viscosity sodium alginate (0.9% w/v) treated in a) Ar and b) Ar/air at different powers: (●) control, (●) 35 W, (●) 45 W, and (●) 55 W.

III. ^{1}H NMR spectra

Liquid-state NMR spectra of alginate solutions were obtained as support measurements for UV-Vis results. Unlike chitosan, sodium alginate has five carbons bound to five hydrogen atoms creating C−H linkages (see fig. 3.8). The sixth carbon outside the ring structure forms an extra double bond with oxygen. Four oxygen atoms create hydroxyl groups, and, unlike the prior, no methyl groups are present.

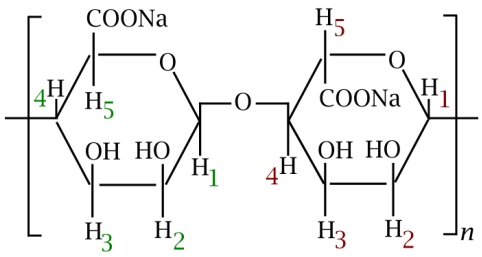

Figure 3.8: Proton ordering of mannuronate (●) and guluronate (●) unit in the sodium alginate copolymer.

Fig. 3.9 shows ^{1}H NMR spectra of untreated and plasma-treated low-viscosity sodium alginate solutions in D_2O. Detected positions of ^{1}H signals in D_2O are summarized in tab. 3.3 according to [147]. Almost all bands were identified in correspondence to ten ^{1}H resonances of mannuronate (M) and guluronate (G) unit blocks. The G5 signal referenced to the position of 4.883 ppm is probably overlapped by the D_2O signal at 4.79 ppm. Two signals with the highest chemical shifts of 5.39 ppm and 5.00 ppm were assigned to G1 and M1, respectively, because of the strongest deshielding by two adjacent oxygen atoms [147].

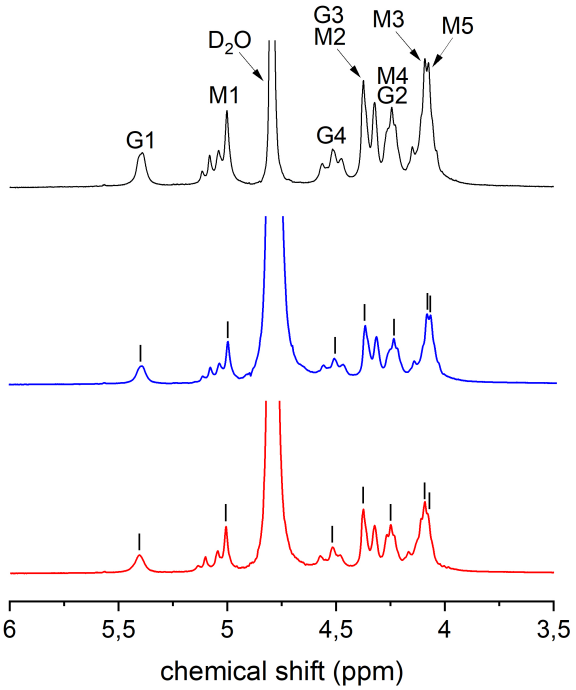

Figure 3.9: ^{1}H NMR spectrum of low-viscosity sodium alginate: (●) control, (●) treated in Ar, and (●) treated in Ar/air for 32 min in D_2O at 330 K.

^{1}H signal	δ (ppm)
G 1	5.39
G 2	4.24
G 3	4.38
G 4	4.52
M 1	5.00
M 2	4.38
M 3	4.09
M 4	4.24
M 5	4.08
D_2O (solvent)	4.79

Table 3.3: Proton chemical shifts δ of sodium alginate in D_2O at 330 K.

To investigate the possible chain transformation of low-viscosity sodium alginate treated by APPJ, the M/G ratio was calculated from the G 1 and M 1 integral intensities, such as

$$\mathrm{M/G_{control}} = \frac{\mathrm{I_{M\ 1}}}{\mathrm{I_{G\ 1}}} = \frac{38.9}{28.0} = 1.4 \tag{3.2}$$

$$\mathrm{M/G_{Ar}} = \frac{\mathrm{I_{M\ 1}}}{\mathrm{I_{G\ 1}}} = \frac{53.7}{22.9} = 2.3 \tag{3.3}$$

$$\mathrm{M/G_{Ar/air}} = \frac{\mathrm{I_{M\ 1}}}{\mathrm{I_{G\ 1}}} = \frac{35.7}{32.5} = 1.1 \tag{3.4}$$

A significant increase in the M/G ratio after Ar treatment compared to the control sample was observed. On the other hand, adding air to Ar plasma resulted in a slight decrease in the M/G ratio. According to the theory of hydrogels, the gel-forming properties of alginate are determined by the proportion and length of poly-G blocks. Alginates with M/G $<$ 1 (higher values of G-blocks) form strong and rigid gels, whereas alginates with M/G $>$ 1 (low values of G-blocks) produce soft and elastic gels [148]. Although there are not many works showing the influence of different M/G ratios on *films'* properties, we may conclude that during the SPP treatment in pure Ar, the polymer degradation predominates the crosslinking mechanism, whereas the air admixture might provoke the formation of a denser network.

3.1.3 Characterization of alginate foils

I. ATR-FTIR spectra

Fig. 3.10 shows ATR-FTIR spectra of low and medium-viscosity alginate films treated in Ar and Ar/air plasma (the treatment was held in the liquid state). The spectra are very similar and agree with those published for alginate elsewhere ([149],[150]). The strong band at 1026 $\mathrm{cm^{-1}}$ [151] might correspond either to O–H bending or the asymmetric stretch of C–O–C; as their absorption bands are close to each other, an overlap might occurred. A weak peak 816 $\mathrm{cm^{-1}}$ is characteristic of mannuronic acid residue. The close-lying bands in the spectral positions of 1080 $\mathrm{cm^{-1}}$, 1124 $\mathrm{cm^{-1}}$, and 1173 $\mathrm{cm^{-1}}$ were attributed to C–O–C,

C−C, and C−O symmetric stretching, respectively. A medium-sharp band at 1408 cm^{-1} and a very strong-sharp peak at 1600 cm^{-1} correspond to symmetric and asymmetric COO^- stretching, respectively. An emerging signal at 2360 cm^{-1} was ascribed to CO_2 vibrations. The band at 2940 cm^{-1} was attributed to C−H stretching. The O−H stretching with a strong shoulder at 3250 cm^{-1} and a broad band in the region from 3280 cm^{-1} to 3380 cm^{-1} were also identified.

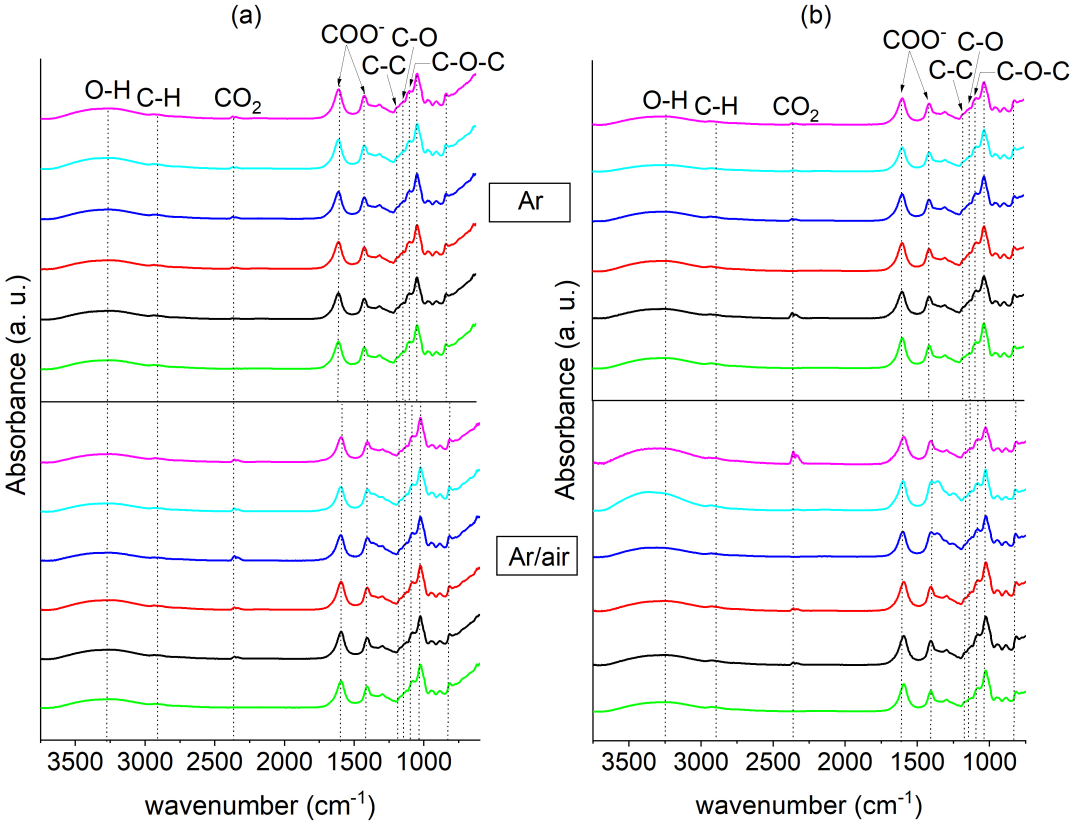

Figure 3.10: ATR-FTIR spectrum of a) low and b) medium-viscosity sodium alginate films treated in Ar and Ar/air with different treatment times: (●) control, (●) 4 min, (●) 8 min, (●) 16 min, (●) 32 min, and (●) 48 min.

At first glance, the FTIR-ATR analysis did not show a measurable change in the chemical structure of plasma-treated alginate, even at high treatment times. However, according to the UV-Vis results, the action of plasma should modify the polymer's chain structure. According to the UV-Vis results, we should expect ester O=C−O−R and carboxyl O=C−O−H bonds with the most intensive peaks of low-viscosity samples treated in Ar and Ar/air at high treatment times (fig. 3.6). Following the theory, the absorption region for C=O and C=C takes from 1500 to 1800 cm^{-1} [131]. The C=C stretching of unconjugated linear alkenes shows moderate to weak absorption in the region of 1640 - 1667 cm^{-1}. The carbonyl groups of aldehydes absorb near 1720 - 1740 cm^{-1}, whereas the C=O band of saturated aliphatic esters absorb in the range of 1735 - 1750 cm^{-1}.

The subtle differences between the FTIR spectra can be distinguished after subtracting the control spectrum from the spectrum of alginate treated by AAPJ in Ar/air (fig. 3.11). The subtraction yields peaks at 1579 cm^{-1} and 1601 cm^{-1}, assigned to the asymmetric COO^- stretching, and at 1735 cm^{-1} and 1732 cm^{-1}, assigned to the C=O ester groups, at high treatment times.

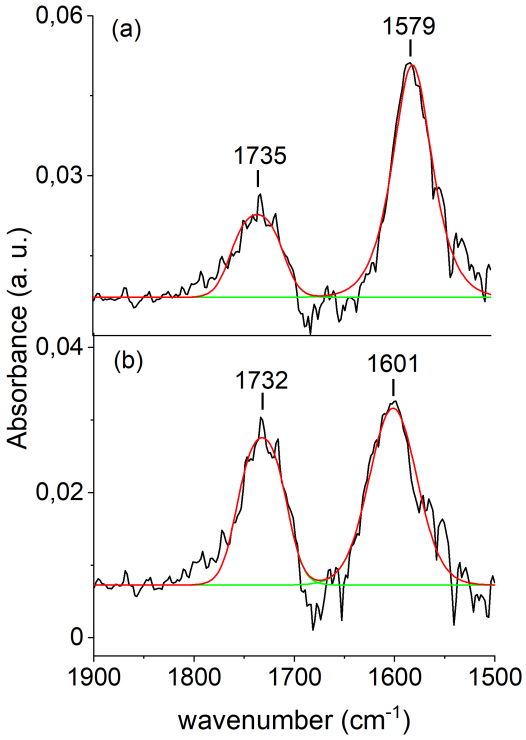

Figure 3.11: The residual spectrum obtained by subtracting the control spectrum from the a) 32 min and b) 48 min treated spectrum of low-viscosity alginate in Ar/air. Gaussian/Lorentz fit was used.

In coherence with studies on chitosan degradation upon SPP treatment [106], this fact confirms the occurrence of secondary oxidation reactions simultaneously with the destruction of alginate chains on APPJ treatment. No C=C bands were observed in the residual spectra.

II. Nanoscale dynamic mechanical analysis

The influence of APPJ treatment on the mechanical properties of alginate films, namely storage modulus G' and loss modulus G", are presented in tab. 3.4. The results of the hardness H are summarized in tab. 3.5

The storage modulus G' was significantly affected by the type of gas used in APPJ. The behavior differs for low and medium-viscosity samples. When low-viscosity alginate films are prepared from solutions exposed to plasma, their storage modulus increases, which is more severe for treatment in the presence of air. The storage modulus of medium-viscosity alginate decreases with applied plasma. For all samples, G' is an order of magnitude higher than G", demonstrating that the elastic component strongly prevails over the viscous component. Furthermore, G' increases with frequency; there might be a similar trend for G", but its values are too small to make decisive conclusions.

Sample		G' (GPa)		G" (GPa)	
		0.1 Hz	300 Hz	0.1 Hz	300 Hz
LV	control	2.5 ± 0.3	14.8 ± 2.1	1.2 ± 2.0	3.0 ± 0.7
	Ar 48 min	3.4 ± 1.4	12.9 ± 1.9	1.2 ± 0.5	1.5 ± 1.3
	Ar/air 48 min	5.6 ± 3.6	19.1 ± 3.4	unreliable	unreliable
MV	control	5.0 ± 1.2	12.7 ± 0.6	unreliable	1.2 ± 0.6
	Ar 48 min	3.6 ± 0.7	13.0 ± 0.9	1.4 ± 2.8	0.6 ± 1.0
	Ar/air 48 min	2.5 ± 0.3	10.3 ± 0.7	1.4 ± 1.5	1.8 ± 0.3

Table 3.4: The results of loss G" and storage G' modulus of alginate foils cast from plasma solution processes.

Considering the hardness, low-viscosity alginate film treated in Ar/air for 48 min is the hardest, whereas medium-viscosity film treated in Ar/air and came as the softest sample. The difference in G' and hardness is almost two-fold.

Sample		H (MPa)	
		0.1 Hz	300 Hz
LV	control	120 ± 90	600 ± 50
	Ar 48 min	70 ± 10	590± 40
	Ar/air 48 min	90 ± 20	840 ± 110
MV	control	70 ± 5	530 ± 30
	Ar 48 min	60 ± 10	460± 20
	Ar/air 48 min	100 ± 50	460 ± 40

Table 3.5: The results of hardness H of alginate foils cast from plasma solution processes.

III. Surface topography

The surface topography measured by AFM of control and plasma-treated alginate films before the tip indentation is shown in fig. 3.12. A significant increase in the surface roughness of alginate foils is observed, especially after Ar treatment (see tab. 3.6). A similar trend is observed for both low and medium-viscosity alginate.

It seems that Ar plasma acts as a more destructive rather than reactive medium compared to plasma with air admixture. The reason might be connected to the velocity of the linking process. High-energetic Ar ions often break simple C–C and C–H bonds enabling free radicals to create random intermolecular junctions. The leakage and the formation of junctions are usually very fast simultaneous processes; however, forming a new junction requires the presence of radicals. In accordance with the results of DSV for low-viscosity alginate (fig. 3.2), chain fragmentation predominates in the first minutes of Ar treatment. Hence, the increased density of diffused polymer fragments results in a more porous structure by no means of creating a polymer network.

On the other hand, it has been reported that the admixture of air into the argon increases the concentration of radicals (e.g., OH, H_2O_2, and NO_2^-) [152]. Combining a lower energy input and a higher concentration of radicals should

lead to a less porous and mechanically stable structure. The chains might re-polymerize in different and more suitable positions with a sufficient density of radicals. Thus, the mechanical performance of polymer films depends not only on the nature of bonds during their formation via APPJ treatment and chain crosslinking but also on the plasma source.

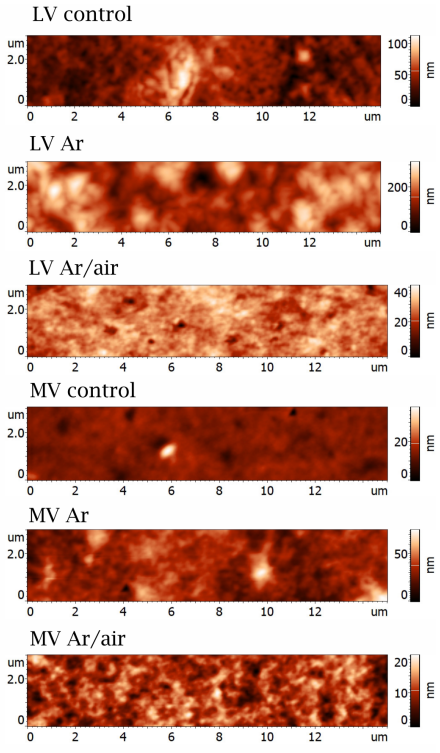

Figure 3.12: Surface topography of low and medium-viscosity alginate foils treated with Ar and Ar/air for 32 min before the indentation by the Berkovich tip.

Sample		RMS roughness (nm)
LV	control	17.0
	Ar 32 min	47.0
	Ar/air 32 min	4.2
MV	control	2.3
	Ar 32 min	9.0
	Ar/air 32 min	3.1

Table 3.6: RMS roughness of plasma-functionalized alginate foils before indentation by the Berkovich tip.

IV. Solubility tests

To study the effect of plasma on the chain cross-linking, a solubility test was performed. Control and plasma-treated alginate foils (1.5×1.5 cm) were immersed in 10 mL of distilled water. The process was filmed on the camera. The period of total dissolution was calculated as a qualitative estimation of the degree of cross-linking. The dissolution times are indicated in tab. 3.7.

Sample	Dissolution time (s)
control	1 s
Ar 48 min	7 s
Ar/air 48 min	> 1 min

Table 3.7: Dissolution time of control and APPJ medium-viscosity alginate foils.

According to theory, a decisive property of polymer networks is their non-solubility in suitable solvents. Although the foil treated in air admixture did not maintain the same shape and water content (due to massive absorption from the solvent) after being immersed in liquid, it withstood a mechanical manipulation after 1 min of soaking. This simple test thus supports the idea of a high degree of crosslinking (a percentage of polymer chains interconnected in the network) induced by APPJ in air admixture.

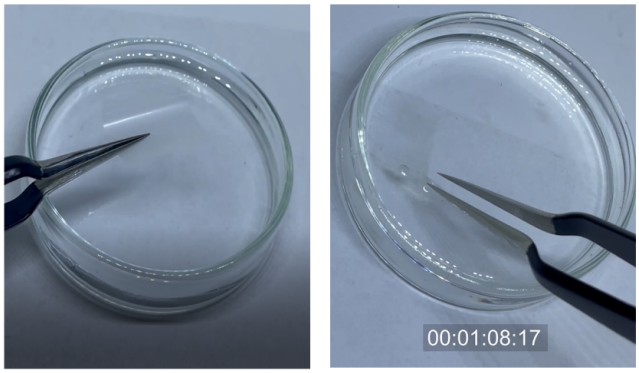

(a) (b)

Figure 3.13: The solubility test of alginate foil treated in Ar/air for 48 min: a) before water plunging, b) manipulation after 1 min of soaking.

3.1.4 Understanding the influence of plasma on alginate properties

To conclude, two main factors have a significant influence on alginate properties: 1) the type of working gas used during solution processing and 2) the density of polymer chains during solution treatment. For understanding the processes induced by plasma, different explanations should be proposed for all cases - low and medium-viscosity alginate, treated in Ar and Ar/air.

Low-viscosity alginate treated in pure Ar plasma evinced an immediate decrease in molar mass with a continual increase afterward. This behavior demonstrates the polymer degradation followed by the re-polymerization process. From the UV-Vis spectra analysis, the concentration of C=O carbonyl bonds significantly increased with increasing treatment time. The increase in M/G ratio calculated from the NMR spectra suggests, that Ar plasma induces a higher concentration of M-blocks in the polymer structure. In addition, an extreme increase in surface roughness was observed for low-viscosity alginate treated in pure Ar. Finally, the solubility tests rejected the possibility of a polymer network formation. According to the observations, a possible model demonstrating the

modifications occurring on the micro-structural level was constructed (see fig. 3.15).

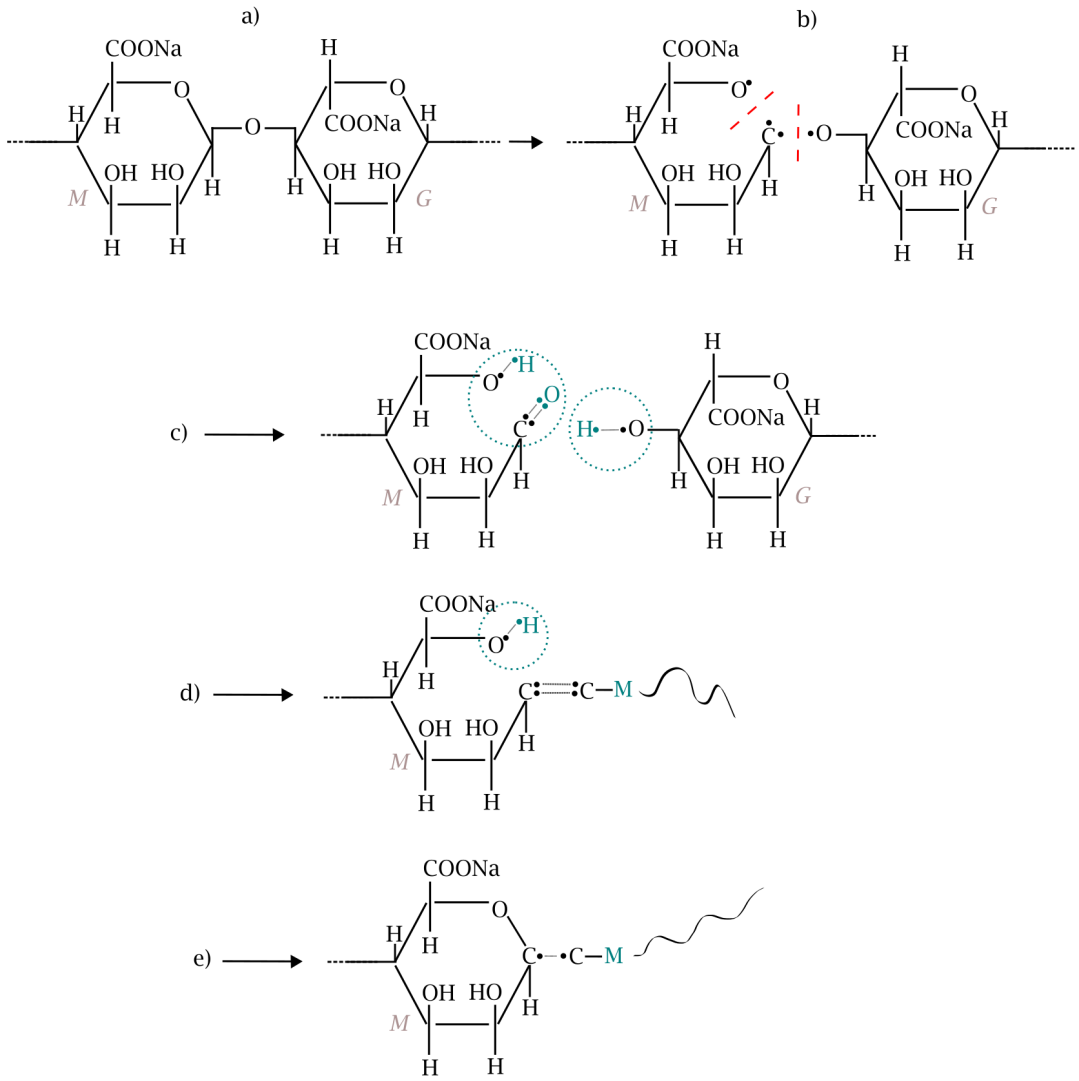

Figure 3.14: Possible chemical pathways occurring in the structure of low-viscosity sodium alginate processed in pure Ar plasma: a) the initial alginate copolymer composed of alternating M and G-blocks, b) scission of the glycosidic linkages and pyranose ring structure, c) the degradation of polymer chains resulting in the decrease of the average molar mass; cleavage followed by the formation of C=O carbonyl bonds, d) the formation of C=C bonds with adjacent M-block; the increase in M-blocks, e) the retention of the pyranose ring structure; a more flexible C–C bond is created with an adjacent M-block.

The treatment of low-viscosity alginate in Ar/air draws different conclusions. Compared to pure Ar plasma, the Ar/air environment employs a higher concentration of oxygen and nitrogen species ($O^{\bullet}$, $NO_2^{\bullet}$). Furthermore, Ar/air plasma increases solution temperature leading to solvent evaporation and an increase in polymer chain density. Accordingly, no chain degradation was observed from the viscosimetry measurement. Besides the formation of C=O bonds, a new band appeared assigned to $NO_2^{\bullet}$ species. No increase was observed in the M/G ratio

compared to the control sample. The shear modulus gained maximum value; on the contrary, the AFM measurements indicated the least porous structure of foils. At last, foils treated in Ar/air withstood immersion in water without dissolving. The latter is followed by the assumption that adding air to Ar plasma leads not only to re-polymerization processes but strong chain crosslinking.

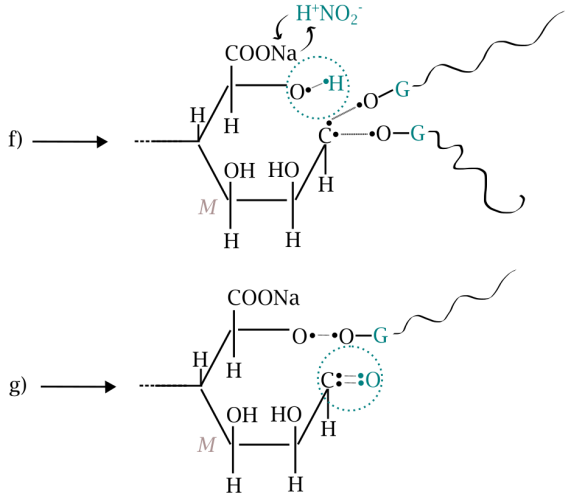

Figure 3.15: Possible chemical pathways occurring in the structure of low-viscosity sodium alginate processed in Ar/air (the mechanism followed by a) and b) from fig. 3.15): f) the increase in branching via glycosidic cleavage followed by the formation of C−O bonds; the dissociation of Na ion followed by a chemical exchange with HNO_2^- species, g) the formation of C=O carbonyl bonds and attachment to the adjacent G-block to the pyranose ring.

3.1.5 Alginate foils incorporated with EOs

According to the literature, alginate itself does not demonstrate antibacterial or anti-mold effects. It should be modified by impregnation or grafting of additional bactericidal agents. Synthetic preservatives and metal nanoparticles are questioned to be dangerous due to their toxicity, therefore, we decided to use nature-derived antibacterial additives, such as essential oils.

I. FTIR spectra

The impact of adding essential almond oil on the intensity of spectral bands is shown in fig. 3.16. Similarly, as in the FTIR spectra of the pure low and medium-viscosity alginate without natural additives (fig. 3.10), characteristic vibrations of C−O−C stretching at 1086 cm^{-1}, C−C at 1120 cm^{-1} were identified. The primary peak at 1035 cm^{-1} was ascribed to O−H bending. The two strong absorption bands at 1413 cm^{-1} and 1608 cm^{-1} were ascribed to symmetric and asymmetric COO^- stretching. The band at 2880 cm^{-1}-2940 cm^{-1} corresponds to the C−H stretching, whereas the broadband at 3200 cm^{-1}-3500 cm^{-1} is attributed to the vibrational stretching of the hydroxyl group. Almond oil is rich in many nutrients such as fatty acids, polar lipids, and triglycerides as in volatile organic consitutuents [153]. Fatty acids include carboxyl groups COOH. However, no significant difference in the spectral structure was observed.

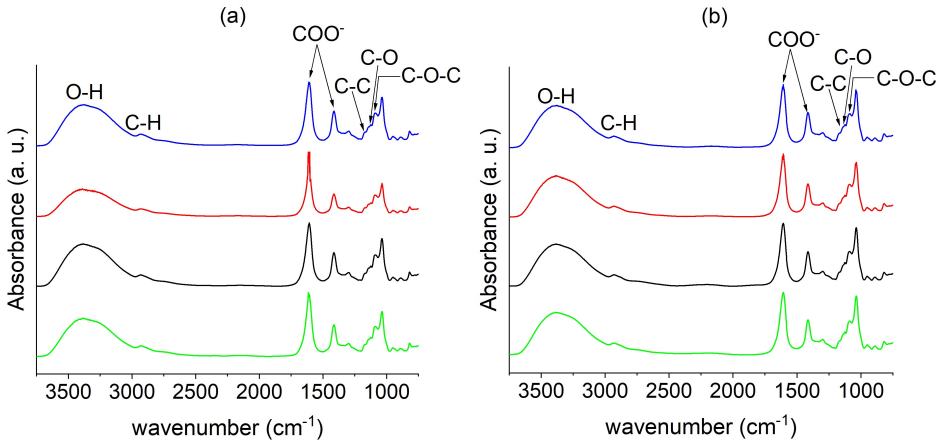

Figure 3.16: FTIR spectrum of a) low and b) medium-viscosity alginate (0.9% w/v) incorporated with 1 mg mL^{-1} of almond oil: (●) control without EO, (●) control with EO, (●) treated in Ar, and (●) treated in Ar/air for 32 min at 35 W.

II. Antibacterial tests

The antibacterial effects of almond essential oil have been studied. In fig. 3.17, the relative viability is represented as an indicator of the metabolic activity of *E. coli* incubated with the control and functionalized alginate foils for 24 h. All results are related to the value one corresponding to the bacteria-positive control.

In the case of Ar plasma, the bactericidal effect of essential oil has been observed, but not so evidently, due to the probably low concentration of oil. However, all three types of samples prepared from Ar/air plasma-processed solution demonstrated perfect antibacterial activity. Essential oil just improved the bactericidal effect. We assume hydrogen peroxide is responsible for the antimicrobial action.

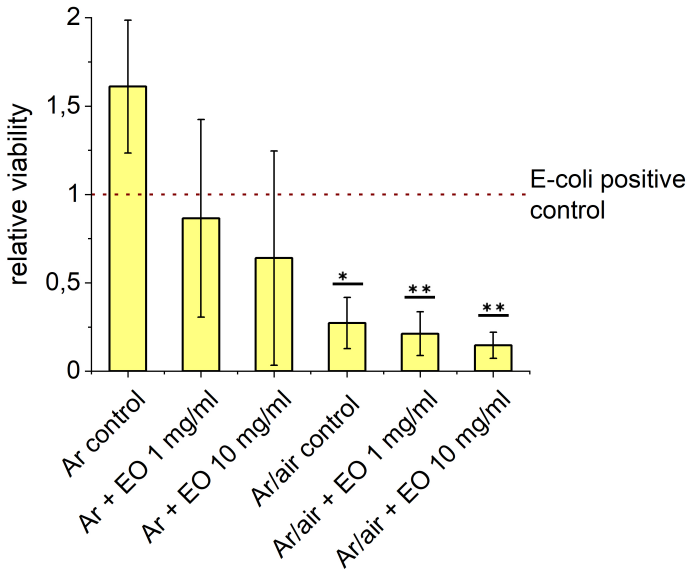

Figure 3.17: Metabolic activity of *E. coli* bacteria after 24 h incubation period on alginate foils with almond essential oil treated with Ar and Ar/air plasma.

To confirm the validity of the results, triplicate statistics should be processed and evaluated. This will be accomplished through further investigation beyond the time scale of experiments related to the diploma thesis.

3.1.6 Using of plasma-processed alginate for food storage

During the storage period, the weight loss in all samples showed an increasing pattern (fig. 3.18). Fruit, especially grapes, contains relatively large amounts of water; when harvested, water loss occurs naturally, and its rate depends on the temperature and relative humidity of the medium [154]. The grapes were stored at $23.7 \pm 0.5\,^{\circ}\mathrm{C}$ temperature and $42.2 \pm 0.5\,\%$ relative humidity in a biological box to maintain equal external conditions.

At the end of 18 days of storage, control grapes lost 49.2% of their initial weight. Even though alginate coatings are considered ineffective in reducing weight loss, several studies indicated improvement with polymer crosslinking [155]. In our case, the weight loss of grapes coated with plasma-treated alginate/EO complex was found efficient. Alginate treated in Ar/air with $10\,\mathrm{mg\,mL^{-1}}$ of almond oil showed the best inhibitory effect towards the weight loss reduction, with a 43.8% weight loss at the end of storage period.

Grapes were inspected every three or four days total of 18 days. During the inspection period, neither a visible lesion nor a fungicidal infected (e.g., gray mold caused by *Botrytis cinerea Pers.*, a direct cause of postharvest decay for table grapes) area was observed in either of the experiments. The only visual decay was attributed to the shrinkage of fruit skin and fruit wilting due to significant weight loss. The shelf life of fruits remained intact until the sixth day of the storage period.

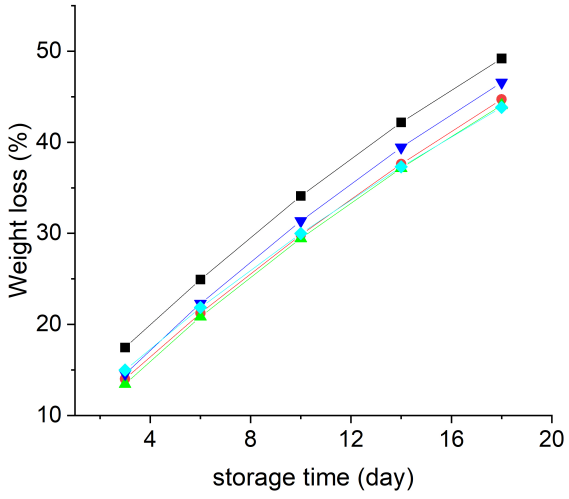

Figure 3.18: Effects of plasma-treated alginate/EO complex coating on weight loss rates of grapes during 18 days of storage: (■) control, (●) Ar + 1 mg/mL EO, (▲) Ar + 10 mg/mL EO, (▼) Ar/air + 1 mg/mL EO, and (◆) Ar/air + 10 mg/mL EO.

Ar	Ar	Ar/air	Ar/air	control
1 mg/mL	10 mg/mL	1 mg/mL	10 mg/L	

Figure 3.19: Day 1: the visual appearance of sprayed and controlled grapes at the beginning of the 18 days storage period.

Ar	Ar	Ar/air	Ar/air	control
1 mg/mL	10 mg/mL	1 mg/mL	10 mg/mL	

Figure 3.20: Day 18: the visual appearance of sprayed and control grapes at the end of the 18 days storage period.

It is important to note, that all berries were washed and UV-sterilized for 10 min before the storage period. Despite the short time of sterilization, this precaution had a strong impact on the grapes' shelf life. The surface of the grapes was probably sterilized to such an extent that no infection occurred event after 26 days in either of the samples. Combining this effect with storage in the biological box was a complete prevention from contact with a pathogenic environment. For future experiments, these conditions should be moderated to guarantee a better imitation of real-life conditions.

Considering the outcome, better results are anticipated when replacing the spraying technique with fruit dipping in the solution. The dipping of berries should ensure a homogeneous layer of coating on the fruits' surface. However, the procedure is time-consuming and less economical.

3.2 Production of water-soluble chitosan by solution plasma system

In the agricultural context, chitosan is emerging as a potential agent used in the defense mechanism of plants, as a growth promoter, antimicrobial agent, or as a safety protection of edible products [156]. Regarding the use of fertilizers, the solubility of chitosan in acidic solutions is an undesirable effect.

Low-temperature atmospheric plasma is a common technique used for polymer surface treatment. Non-thermal atmospheric plasma produces reactive species activating polymers' surfaces. Chitosan was already shown to undergo structural modifications in solution plasma processes [157]. The exposure of biopolymer samples to radicals leads to the breakage of chemical bonds and thus results in the degradation of polymer chains. As concluded in many studies, lowering the molecular weight helps to improve chitosan's solubility.

Chitosan solution (1% w/v acetic acid) was processed using DC glow discharge in contact with liquid by the group in G. A. Krestov Institute of Solution Chemistry of RAS. Then, water-soluble and water-insoluble fractions were separated, dried, and studied in form of powders. The structural analysis of the powders was performed in the frame of this diploma thesis.

3.2.1 Molar mass distribution

The main effect of plasma on chitosan's structure is its degradation - the creation of low-molecular-weight species, so-called oligomers. This phenomenon was analyzed by Gel permeation chromatography resulting in a molar mass distribution of control and plasma-processed β-chitosan.

Fig. 3.21 shows the molar mass distribution of control and plasma-treated chitosan fractions measured with columns of different porosity. For the untreated sample, a weak signal at 300 kDa was observed, corresponding to high-molecular-weight components (fig. 3.21a). This signal was assigned to the initial molar mass of chitosan. For the water-soluble fraction, a wider distribution in a range of 75 - 410 kDa was observed, due to running degradation processes; all high-molecular-weight components were dissolved in the case of insoluble fraction, with no signal detected.

Water-soluble and insoluble fractions were not dissolved properly in THF, thus the GPC measurements are not ideal. However, low-molecular-weight fragments, contained also in the untreated sample, were successfully dissolved (fig. 3.21b) and detected at 0.3 kDa for all three samples. The distribution of control chitosan evinces, in comparison with the irradiated samples, a multimodal character. The presence of secondary modes ((0.6 kDa and 1.1 kDa) is often related to the branching of polymer chains. The attenuation and further disappearance of secondary peaks of water-soluble and insoluble fractions, respectively, indicate a favorable effect of plasma treatment upon chitosan degradation.

Hence, the absence of high-molecular-weight components and attenuation of secondary modes in the case of plasma-treated chitosan fractions suggest biopolymer destruction under the action of the non-thermal plasma resulting in chain breaking.

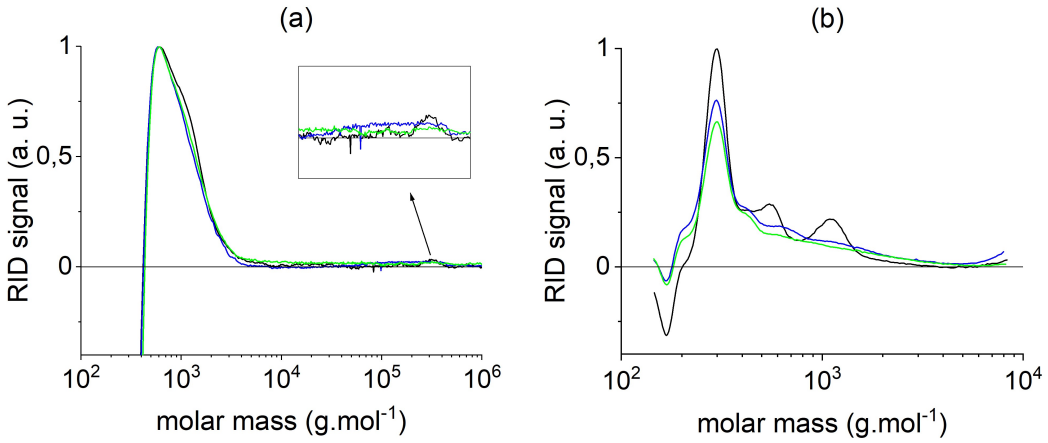

Figure 3.21: Molar mass distribution of chitosan detected by GPC: (●) control, (●) water-soluble, and (●) insoluble fraction. PLGEL column of different porosity was used: a) 10 000 L/5 µm and b) 100 L/5 µm, with the THF flow rate 0.8 mL min^{-1} at 30 °C.

3.2.2 ^{1}H NMR spectra

The chemical composition of control and plasma-treated β-chitosan fractions in D_2O/DCl and D_2O was studied by liquid-state NMR spectroscopy. Each unit residue of the copolymer has six carbon and seven hydrogen atoms producing C–H linkages and four hydrogens atoms bound to oxygen, creating O–H bonds (for notation see fig. 3.22). In addition, the acetylglucosamine units consist of one methyl group. The positions of ^{1}H signals in D_2O/DCl and D_2O are summarized in tab. 3.9 and tab. 3.8, respectively, according to [158].

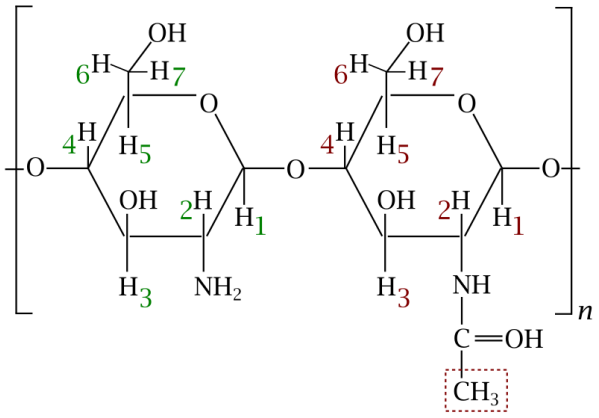

Figure 3.22: Proton ordering of the glucosamine (left) and acetylglucosamine (right) units of chitosan.

Fig. 3.23 shows ^{1}H NMR spectra of chitosan dissolved in D_2O/DCl without and under the action of plasma for 32 min. DCl is considered a suitable solvent for chitosan, which is confirmed by the presence of ^{1}H signals even in the untreated NMR spectrum. This is a typical ^{1}H NMR solution spectrum of chitosan with signals at 2.1 ppm assigned to acetylated methyl protons (A CH_3), the protons in the pyranose ring (A/G H3-6), and two signals at 3.2 ppm and 4.9 ppm

corresponding to the H-1, and H-2 glucosamine units (G H1, G H2). ^{1}H NMR spectrum of chitosan soluble fraction gives us complete information on the chemical structure of the plasma-treated sample. Compared with untreated chitosan, acetylated methyl protons (A CH3) intensity significantly decreases with plasma treatment. For the plasma-treated samples, the band at 8.5 ppm was assigned to the pyranose ring's protonated primary amines NH_3^+ [106].

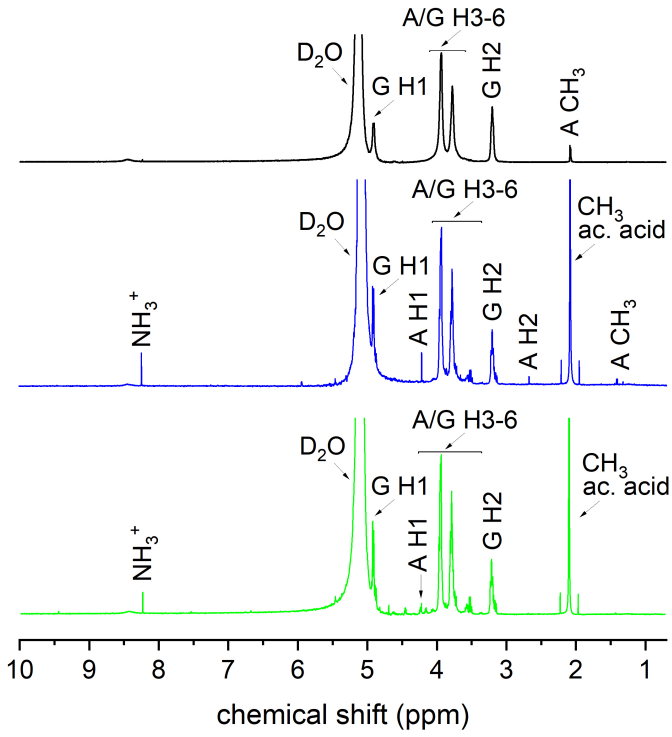

Figure 3.23: ^{1}H NMR spectrum of β-chitosan: (●) control, (●) water-soluble, and (●) insoluble fraction in D_2O/DCl at 298 K.

^{1}H signal	δ (ppm)
A CH_3	1.4
CH_3 acetic acid	2.0
A H2	2.7
G H2	3.2
A/G H3-6	3.4 - 4.1
A H1	4.2
G H1	4.9
D_2O (solvent)	5.2
NH_3^+	8.2

Table 3.8: Proton chemical shifts δ of chitosan water-soluble and insoluble fractions in D_2O/DCl at 298 K.

Up to the present, no successful measurement with a high peak resolution of the ^{1}H NMR spectrum in pure D_2O has been published due to poor chitosan solubility. In this study, the spectrum of chitosan plasma-treated water-soluble

fraction was successfully measured and analyzed (fig. 3.24). As expected, in the spectrum of untreated chitosan only the solvent's signal at 4.8 ppm was detected. On the contrary, for the plasma-treated soluble fraction, almost all bands were identified. The H-1 band of glucosamine chitosan was not observed, probably due to overlap with the strong solvent's signal. The acetylglucosamine H-1 signal (A H1) was detected at 4.5 ppm. The internal (non-anomeric) protons connected to the ring skeleton in both A and G-block residues have similar electron densities and thus have similar chemical shifts [158]. These signals partially overlap and produce a broad envelope in a range of 3.3-4.0 ppm of proton signals (A/G H3-6). Compared to the spectrum measured in D_2O/DCl, dissolving chitosan in water provides better resolution of the pyranose ring signals. The employment of plasma upon the chitosan modification enlarges the observation techniques and possibilities for a better understanding of plasma-enhanced micro-structural mechanisms.

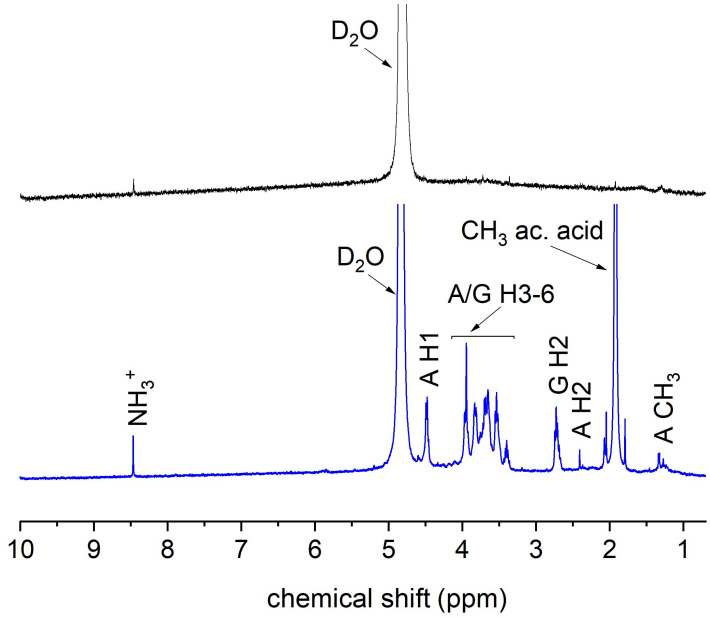

Figure 3.24: ^{1}H NMR spectrum of β-chitosan: (●) control and (●) water-soluble fraction in D_2O at 298 K.

^{1}H signal	δ (ppm)
A CH_3	1.1 - 1.4
CH_3 acetic acid	1.7 - 2.1
A H2	2.4
G H2	2.7
A/G H3-6	3.3 - 4.0
A H1	4.5
D_2O (solvent)	4.8
NH_3^+	8.5

Table 3.9: Proton chemical shifts δ of chitosan water-soluble and insoluble fractions in D_2O at 298 K.

The experimental results indicate that the chemical composition of chitosan is not affected by the solution plasma treatment. Supported by the work of *Khlyustova et al.*, the only changes induced by solution plasma were related to the formation of double bonds and weakening of inter- and intramolecular hydrogen bonds [157].

To investigate the structural modifications of chitosan after the action of plasma, the degree of deacetylation (DD) was calculated using the integral area of the proton H-2 of the glucosamine unit (G H2) and of the peak of three protons of the acetyl group (A CH_3)

$$\mathrm{DD}(\%) = \frac{\mathrm{I_{G\ H2}}}{\mathrm{I_{G\ H2}} + \frac{1}{3}\mathrm{I_{A\ CH_3}}} \cdot 100\%. \tag{3.5}$$

This approach is a slight modification of the technique proposed by *Lavertu et al.* [159], who suggested calculation from H-1 signals of glucosamine unit (G H1); however, these signals are not visible in the D_2O spectrum and overlap with the solvent's signal in the D_2O/DCl spectra. The results of DD calculated for the chitosan water-soluble fraction measured in D_2O/DCl and D_2O, respectively, are as follows

$$\mathrm{DD_{D_2O/DCl}} = 98\%, \tag{3.6}$$

$$\mathrm{DD_{D_2O}} = 87\%. \tag{3.7}$$

DD is an important factor affecting the structural and mechanical properties. It has been reported that increasing DD induces higher elongation at break and water content [160]. Compared to the DD given by the producer, $\sim$ 82%, the plasma treatment increases the ratio of the glucosamine units, especially for the measurement in DCl. Evidently, the acidic environment influences the final structure of the biopolymer. Even though the results come in contradiction in relation to the mechanical properties, the increase in the DD after plasma treatment is in coherence with the study of *Nikitin et al.*. For the plasma-treated samples, the appearance of the protonated primary amines (NH_3^+) documents the additional deacetylation occurring by the influence of the plasma [106].

Conclusion

The aims of this thesis were successfully met as follows:

- Atmospheric pressure plasma jet has been demonstrated as a versatile tool for the modification of sodium alginate in aqueous solution. The effects of plasma treatment on the physicochemical properties of alginate have been investigated by viscosimetry, UV-Vis, and NMR spectroscopy. Differences in the temporal evolution of molecular weight as well as in the chemical composition of solution were observed for different plasma-forming gases.

- Plasma-processed alginate solutions were successfully used for the casting of foils with advanced properties. According to the results of FTIR spectroscopy, AFM, and nanoindentation, the addition of air admixture to Ar significantly influences the final structure of alginate. It is hypothesized that Ar plasma mostly breaks the glucosidic bonds leading to a drastic change in the M/G ratio as was confirmed by NMR. The resulting foils are rough and porous. The admixture of air to Ar initiates the disruption of C−O−C bonds in the pyranose ring promoting the further formation of a highly cross-linked structure. The resulting foils are smooth and dense.

- It was surprising to obtain the antibacterial alginate foils by Ar/air plasma treatment without the addition of bactericidal agents. The hypothesis of this phenomenon is the release of hydrogen peroxide formed in solution during the plasma processing and became embedded into foils during their fabrication.

- Impregnation of alginate foils with almond essential oil to alginate foils improves their antibacterial performance for both types of plasma treatment.

- A promising effect of alginate coatings toward preserving table grapes' quality and extending fruits' shell life was revealed. The results showed a measurable delay in weight loss.

- The chemical composition and structural properties of untreated, water-soluble, and water-insoluble chitosan fractions were analyzed using combined information from GPC and NMR. According to the results, plasma action does not affect the chemical composition of chitosan but leads to its degradation.

- ^{1}H NMR spectrum of the water-soluble fraction of chitosan in pure D_2O was acquired. In contrast, chitosan signals were not detected in the case of untreated samples. This is great evidence of the successful fabrication of chitosan oligomers soluble in water using a plasma solution system, which might be promising for use as fertilizers for agricultural applications.

Bibliography

[1] Giuseppe Mensitieri, Ernesto Di Maio, Giovanna G Buonocore, Irma Nedi, Maria Oliviero, Lucia Sansone, and Salvatore Iannace. Processing and shelf life issues of selected food packaging materials and structures from renewable resources. *Trends in Food Science & Technology*, 22(2-3):72–80, 2011.

[2] Statista. Plasticseurope (pemrg). annual production of plastics worldwide from 1950 to 2020 (in million metric tons) [graph]. 2022.

[3] Statista. Basel convention. distribution of plastic waste treatment worldwide in 2018, by method [graph]. 2022.

[4] Camila Távora de Mello Soares, Monica Ek, Emma Östmark, Mikael Gällstedt, and Sigbritt Karlsson. Recycling of multi-material multilayer plastic packaging: Current trends and future scenarios. *Resources, Conservation and Recycling*, 176:105905, 2022.

[5] Richard C Thompson, Ylva Olsen, Richard P Mitchell, Anthony Davis, Steven J Rowland, Anthony WG John, Daniel McGonigle, and Andrea E Russell. Lost at sea: where is all the plastic? *Science*, 304(5672):838–838, 2004.

[6] Jiao Wang, Xianhua Liu, Yang Li, Trevor Powell, Xin Wang, Guangyi Wang, and Pingping Zhang. Microplastics as contaminants in the soil environment: A mini-review. *Science of the total environment*, 691:848–857, 2019.

[7] Laura N Vandenberg, Russ Hauser, Michele Marcus, Nicolas Olea, and Wade V Welshons. Human exposure to bisphenol a (bpa). *Reproductive toxicology*, 24(2):139–177, 2007.

[8] Shanna H Swan. Environmental phthalate exposure in relation to reproductive outcomes and other health endpoints in humans. *Environmental research*, 108(2):177–184, 2008.

[9] Charles James Moore. Synthetic polymers in the marine environment: a rapidly increasing, long-term threat. *Environmental research*, 108(2):131–139, 2008.

[10] Cai Zhang, Xiaohua Chen, Jiangtao Wang, and Liju Tan. Toxic effects of microplastic on marine microalgae skeletonema costatum: interactions between microplastic and algae. *Environmental pollution*, 220:1282–1288, 2017.

[11] D Michael Fry, Stewart I Fefer, and Louis Sileo. Ingestion of plastic debris by laysan albatrosses and wedge-tailed shearwaters in the hawaiian islands. *Marine Pollution Bulletin*, 18(6):339–343, 1987.

[12] Leandro Bugoni, Lıgia Krause, and Maria Virgınia Petry. Marine debris and human impacts on sea turtles in southern brazil. *Marine pollution bulletin*, 42(12):1330–1334, 2001.

[13] Stephanie L Wright, Richard C Thompson, and Tamara S Galloway. The physical impacts of microplastics on marine organisms: a review. *Environmental pollution*, 178:483–492, 2013.

[14] Statista. Basel convention. distribution of plastic waste generation worldwide in 2018, by sector [graph]. 2022.

[15] Mariana Mazzucato. Mission-oriented research & innovation in the european: a problem-solving approach to fuel innovation-led growth. 2018.

[16] Ali Chamas, Hyunjin Moon, Jiajia Zheng, Yang Qiu, Tarnuma Tabassum, Jun Hee Jang, Mahdi Abu-Omar, Susannah L Scott, and Sangwon Suh. Degradation rates of plastics in the environment. *ACS Sustainable Chemistry & Engineering*, 8(9):3494–3511, 2020.

[17] Y Murata, N Sasaki, E Miyamoto, and S Kawashima. Use of floating alginate gel beads for stomach-specific drug delivery. *European journal of pharmaceutics and biopharmaceutics*, 50(2):221–226, 2000.

[18] Meera George and T Emilia Abraham. Polyionic hydrocolloids for the intestinal delivery of protein drugs: alginate and chitosan—a review. *Journal of controlled release*, 114(1):1–14, 2006.

[19] Bahareh Saberi, Rahul Thakur, Deep Jyoti Bhuyan, Quan V Vuong, Suwimol Chockchaisawasdee, John B Golding, Christopher J Scarlett, and Costas E Stathopoulos. Development of edible blend films with good mechanical and barrier properties from pea starch and guar gum. *Starch-Stärke*, 69(1-2):1600227, 2017.

[20] Tooraj Mehdizadeh, Hossein Tajik, Ali Mojaddar Langroodi, Rahim Molaei, and Alireza Mahmoudian. Chitosan-starch film containing pomegranate peel extract and thymus kotschyanus essential oil can prolong the shelf life of beef. *Meat science*, 163:108073, 2020.

[21] You Luo, Haiqing Liu, Shanzhong Yang, Jiarui Zeng, and Zhenqiang Wu. Sodium alginate-based green packaging films functionalized by guava leaf extracts and their bioactivities. *Materials*, 12(18):2923, 2019.

[22] K Madhumathi, Sudheesh Kumar, S Abhilash, V Sreeja, H Tamura, K Manzoor, SV Nair, and R Jayakumar. Development of novel chitin/nanosilver composite scaffolds for wound dressing applications. *Journal of Materials Science: Materials in Medicine*, 21(2):807–813, 2010.

[23] Paul H Weigel, Vincent C Hascall, and Markku Tammi. Hyaluronan synthases. *Journal of Biological Chemistry*, 272(22):13997–14000, 1997.

[24] Mathew Peter, NS Binulal, SV Nair, N Selvamurugan, H Tamura, and R Jayakumar. Novel biodegradable chitosan–gelatin/nano-bioactive glass ceramic composite scaffolds for alveolar bone tissue engineering. *Chemical engineering journal*, 158(2):353–361, 2010.

[25] Elsie S Place, Nicholas D Evans, and Molly M Stevens. Complexity in biomaterials for tissue engineering. *Nature materials*, 8(6):457–470, 2009.

[26] Hyun Gyu Park, Tae Won Kim, Myeong Yun Chae, and Ik-Keun Yoo. Activated carbon-containing alginate adsorbent for the simultaneous removal of heavy metals and toxic organics. *Process Biochemistry*, 42(10):1371–1377, 2007.

[27] Ming-Shen Chiou, Pang-Yen Ho, and Hsing-Ya Li. Adsorption of anionic dyes in acid solutions using chemically cross-linked chitosan beads. *Dyes and pigments*, 60(1):69–84, 2004.

[28] Ke Xing, Xiao Zhu, Xue Peng, and Sheng Qin. Chitosan antimicrobial and eliciting properties for pest control in agriculture: a review. *Agronomy for Sustainable Development*, 35(2):569–588, 2015.

[29] Mohammad A Chowdhury. The controlled release of bioactive compounds from lignin and lignin-based biopolymer matrices. *International journal of biological macromolecules*, 65:136–147, 2014.

[30] Florencia Versino, Olivia V Lopez, Maria A Garcia, and Noemi E Zaritzky. Starch-based films and food coatings: An overview. *Starch-Stärke*, 68(11-12):1026–1037, 2016.

[31] José Carlos Rodríguez-Cabello, Francisco Javier Arias, Matilde Alonso Rodrigo, and Alessandra Girotti. Elastin-like polypeptides in drug delivery. *Advanced drug delivery reviews*, 97:85–100, 2016.

[32] Maria Chiara Barsotti, Francesca Felice, Alberto Balbarini, and Rossella Di Stefano. Fibrin as a scaffold for cardiac tissue engineering. *Biotechnology and applied biochemistry*, 58(5):301–310, 2011.

[33] Petr Snetkov, Kseniia Zakharova, Svetlana Morozkina, Roman Olekhnovich, and Mayya Uspenskaya. Hyaluronic acid: The influence of molecular weight on structural, physical, physico-chemical, and degradable properties of biopolymer. *Polymers*, 12(8):1800, 2020.

[34] AC Albertsson and S Karlsson. Chemistry and technology of biodegradable polymers. *Blackie. Glasgow*, 48, 1994.

[35] Sanjay K Sharma and Ackmez Mudhoo. *A handbook of applied biopolymer technology: synthesis, degradation and applications*. Royal society of chemistry, 2011.

[36] K Madhavan Nampoothiri, Nimisha Rajendran Nair, and Rojan Pappy John. An overview of the recent developments in polylactide (pla) research. *Bioresource technology*, 101(22):8493–8501, 2010.

[37] AM Mohan. Danone first to switch to pla for yogurt cup in germany, 2015.

[38] C. Purac. Bioplastics product profile: Pla thermoformed single-use hot beverage cups, corbion, 2013.

[39] Tenova Bioplastics AB. Compostable grocery bags. 2009.

[40] Lakshmi S Nair and Cato T Laurencin. Biodegradable polymers as biomaterials. *Progress in polymer science*, 32(8-9):762–798, 2007.

[41] Eugene D Boland, Todd A Telemeco, David G Simpson, Gary E Wnek, and Gary L Bowlin. Utilizing acid pretreatment and electrospinning to improve biocompatibility of poly (glycolic acid) for tissue engineering. *Journal of Biomedical Materials Research Part B: Applied Biomaterials: An Official Journal of The Society for Biomaterials, The Japanese Society for Biomaterials, and The Australian Society for Biomaterials and the Korean Society for Biomaterials*, 71(1):144–152, 2004.

[42] Motoki Fujita, Yukihiko Kinoshita, Emiko Sato, Hatsuhiko Maeda, Satoshi Ozono, Hideyuki Negishi, Toshio Kawase, Yosuke Hiraoka, Tomoaki Takamoto, Yasuhiko Tabata, et al. Proliferation and differentiation of rat bone marrow stromal cells on poly (glycolic acid)–collagen sponge. *Tissue engineering*, 11(9-10):1346–1355, 2005.

[43] Lakshmi S Nair and Cato T Laurencin. Polymers as biomaterials for tissue engineering and controlled drug delivery. *Tissue engineering I*, pages 47–90, 2005.

[44] ChangYang Gong, ZhiYong Qian, CaiBing Liu, MeiJuan Huang, YingChun Gu, YanJun Wen, Bing Kan, Ke Wang, Mei Dai, XingYi Li, et al. A thermosensitive hydrogel based on biodegradable amphiphilic poly (ethylene glycol)–polycaprolactone–poly (ethylene glycol) block copolymers. *Smart materials and structures*, 16(3):927, 2007.

[45] Elbadawy A Kamoun, El-Refaie S Kenawy, and Xin Chen. A review on polymeric hydrogel membranes for wound dressing applications: Pva-based hydrogel dressings. *Journal of advanced research*, 8(3):217–233, 2017.

[46] Marguerite Rinaudo. Chitin and chitosan: Properties and applications. *Progress in polymer science*, 31(7):603–632, 2006.

[47] Riccardo AA Muzzarelli, Charles Jeuniaux, Graham W Gooday, et al. *Chitin in nature and technology*, volume 385. Springer, 1986.

[48] Sergio P Campana-Filho, Douglas de Britto, Elisabete Curti, Fernanda R Abreu, Marcia B Cardoso, Marcos V Battisti, Priscilla C Sim, Rejane C Goy, Roberta Signini, and Rodrigo L Lavall. Extraction, structures and properties of alpha-and beta-chitin. *Química Nova*, 30:644–650, 2007.

[49] Youling Yuan, Betsy M Chesnutt, Warren O Haggard, and Joel D Bumgardner. Deacetylation of chitosan: Material characterization and in vitro evaluation via albumin adsorption and pre-osteoblastic cell cultures. *Materials*, 4(8):1399–1416, 2011.

[50] Peter A Williams. *Renewable resources for functional polymers and biomaterials: polysaccharides, proteins and polyesters*. Royal society of chemistry, 2011.

[51] Marguerite Rinaudo. Main properties and current applications of some polysaccharides as biomaterials. *Polymer International*, 57(3):397–430, 2008.

[52] Chennakkattu KS Pillai, Willi Paul, and Chandra P Sharma. Chitin and chitosan polymers: Chemistry, solubility and fiber formation. *Progress in polymer science*, 34(7):641–678, 2009.

[53] Miguel A Ramírez, Aida T Rodríguez, Luis Alfonso, and Carlos Peniche. Chitin and its derivatives as biopolymers with potential agricultural applications. *Biotecnología Aplicada*, 27(4):270–276, 2010.

[54] Lan Wu and Mingzhu Liu. Preparation and properties of chitosan-coated npk compound fertilizer with controlled-release and water-retention. *Carbohydrate polymers*, 72(2):240–247, 2008.

[55] Donald E Clark and Harland C Green. Alginic acid and process of making same, April 7 1936. US Patent 2,036,922.

[56] Kuen Yong Lee and David J Mooney. Alginate: properties and biomedical applications. *Progress in polymer science*, 37(1):106–126, 2012.

[57] Xi Guo, Yan Wang, Yimin Qin, Peili Shen, and Qiang Peng. Structures, properties and application of alginic acid: A review. *International Journal of Biological Macromolecules*, 162:618–628, 2020.

[58] Cheong Hian Goh, Paul Wan Sia Heng, and Lai Wah Chan. Alginates as a useful natural polymer for microencapsulation and therapeutic applications. *Carbohydrate polymers*, 88(1):1–12, 2012.

[59] Roxana Gheorghita Puscaselu, Andrei Lobiuc, Mihai Dimian, and Mihai Covasa. Alginate: From food industry to biomedical applications and management of metabolic disorders. *Polymers*, 12(10):2417, 2020.

[60] Antonio Jiménez-Escrig and FJ Sánchez-Muniz. Dietary fibre from edible seaweeds: Chemical structure, physicochemical properties and effects on cholesterol metabolism. *Nutrition research*, 20(4):585–598, 2000.

[61] Tomoko Shimokawa, Shigeki Yoshida, Toshio Takeuchi, Katsumi Murata, Tadashi Ishii, and Isao Kusakabe. Preparation of two series of oligoguluronic acids from sodium alginate by acid hydrolysis and enzymatic degradation. *Bioscience, biotechnology, and biochemistry*, 60(9):1532–1534, 1996.

[62] Alexander D Augst, Hyun Joon Kong, and David J Mooney. Alginate hydrogels as biomaterials. *Macromolecular bioscience*, 6(8):623–633, 2006.

[63] Jong-Whan Rhim. Physical and mechanical properties of water resistant sodium alginate films. *LWT-Food science and technology*, 37(3):323–330, 2004.

[64] Vianney T Ojerio, Valeriano L Corre, Nieves A Toledo, Karen Grace S Andrino-Felarca, Lovelyn Marie Nievales, and Rex Ferdinand M Traifalgar. Alginic acid as immunostimulant: effects of dose and frequency on growth performance, immune responses, and white spot syndrome virus resistance in tiger shrimp penaeus monodon (fabricius, 1798). *Aquaculture international*, 26(1):267–278, 2018.

[65] Micheline Cristiane Rocha de Souza, Cybelle Teixeira Marques, Celina Maria Guerra Dore, Fernando Roberto Ferreira da Silva, Hugo Alexandre Oliveira Rocha, and Edda Lisboa Leite. Antioxidant activities of sulfated polysaccharides from brown and red seaweeds. *Journal of applied phycology*, 19(2):153–160, 2007.

[66] IP Shanura Fernando, Thilina U Jayawardena, KK Asanka Sanjeewa, Lei Wang, You-Jin Jeon, and Won Woo Lee. Anti-inflammatory potential of alginic acid from sargassum horneri against urban aerosol-induced inflammatory responses in keratinocytes and macrophages. *Ecotoxicology and environmental safety*, 160:24–31, 2018.

[67] Loris Rizzello and Pier Paolo Pompa. Nanosilver-based antibacterial drugs and devices: mechanisms, methodological drawbacks, and guidelines. *Chemical Society Reviews*, 43(5):1501–1518, 2014.

[68] K Husnu Can Baser and Gerhard Buchbauer. *Handbook of essential oils: science, technology, and applications*. CRC press, 2009.

[69] SAAJ Van de Braak and GCJJ Leijten. Essential oils and oleoresins: a survey in the netherlands and other major markets in the european union. *CBI, centre for the promotion of imports from developing countries, Rotterdam*, 116, 1999.

[70] Behzad Moradi, Saeid Heidari-Soureshjani, Majid Asadi-Samani, and Qian Yang. A systematic review of phytochemical and phytotherapeutic characteristics of bitter almond. *International Journal of Pharmaceutical and Phytopharmacological Research*, 7:1–9, 2017.

[71] Brian M Lawrence. The botanical and chemical aspects of oregano. *Perfumer & flavorist*, 9(5):41–51, 1984.

[72] C Lens-Lisbonne, A Cremieux, C Maillard, and G Balansard. Methodes d'evaluation de l'activite antibacterienne des huiles essentielles: application aux essences de thym et de cannelle. *J Pharm Belg*, 42(5):297–302, 1987.

[73] Christine F Carson, Katherine A Hammer, and Thomas V Riley. Melaleuca alternifolia (tea tree) oil: a review of antimicrobial and other medicinal properties. *Clinical microbiology reviews*, 19(1):50–62, 2006.

[74] Hsiu-Fang Yen, Chi-Ting Hsieh, Tusty-Jiuan Hsieh, Fang-Rong Chang, and Chin-Kun Wang. In vitro anti-diabetic effect and chemical component analysis of 29 essential oils products. *journal of food and drug analysis*, 23(1):124–129, 2015.

[75] Vaiyapuri Subbarayan Periasamy, Jegan Athinarayanan, and Ali A Alshatwi. Anticancer activity of an ultrasonic nanoemulsion formulation of nigella sativa l. essential oil on human breast cancer cells. *Ultrasonics sonochemistry*, 31:449–455, 2016.

[76] A Ocana-Fuentes, E Arranz-Gutierrez, FJ Senorans, and G Reglero. Supercritical fluid extraction of oregano (origanum vulgare) essentials oils: anti-inflammatory properties based on cytokine response on thp-1 macrophages. *Food and Chemical Toxicology*, 48(6):1568–1575, 2010.

[77] Regiane Ribeiro-Santos, Mariana Andrade, Nathália Ramos de Melo, and Ana Sanches-Silva. Use of essential oils in active food packaging: Recent advances and future trends. *Trends in food science & technology*, 61:132–140, 2017.

[78] I Atrea, A Papavergou, I Amvrosiadis, and IN Savvaidis. Combined effect of vacuum-packaging and oregano essential oil on the shelf-life of mediterranean octopus (octopus vulgaris) from the aegean sea stored at 4 c. *Food microbiology*, 26(2):166–172, 2009.

[79] Mounia Oussalah, Stephane Caillet, Stéphane Salmiéri, Linda Saucier, and Monique Lacroix. Antimicrobial effects of alginate-based films containing essential oils on listeria monocytogenes and salmonella typhimurium present in bologna and ham. *Journal of food protection*, 70(4):901–908, 2007.

[80] Pablo R Salgado, M Elvira López-Caballero, M Carmen Gómez-Guillén, Adriana N Mauri, and M Pilar Montero. Sunflower protein films incorporated with clove essential oil have potential application for the preservation of fish patties. *Food Hydrocolloids*, 33(1):74–84, 2013.

[81] Kyriaki G Zinoviadou, Konstantinos P Koutsoumanis, and Costas G Biliaderis. Physico-chemical properties of whey protein isolate films containing oregano oil and their antimicrobial action against spoilage flora of fresh beef. *Meat Science*, 82(3):338–345, 2009.

[82] Francis F Chen et al. *Introduction to plasma physics and controlled fusion*, volume 1. Springer, 1984.

[83] Jörg Florian Friedrich and Jürgen Meichsner. *Nonthermal Plasmas for Materials Processing*. John Wiley & Sons, 2022.

[84] Alexander Fridman. *Plasma chemistry*. Cambridge university press, 2008.

[85] Alexander Piel. *Plasma physics: an introduction to laboratory, space, and fusion plasmas*. Springer, 2017.

[86] Paul M Bellan. *Fundamentals of plasma physics*. Cambridge university press, 2008.

[87] Michael A Lieberman and Alan J Lichtenberg. *Principles of plasma discharges and materials processing*. John Wiley & Sons, 2005.

[88] Paul Gibbon. Introduction to plasma physics. *arXiv preprint arXiv:2007.04783*, 2020.

[89] Gregory Fridman, Gary Friedman, Alexander Gutsol, Anatoly B Shekhter, Victor N Vasilets, and Alexander Fridman. Applied plasma medicine. *Plasma processes and polymers*, 5(6):503–533, 2008.

[90] Yu I Davydov. On the first townsend coefficient at high electric field. *IEEE Transactions on Nuclear Science*, 53(5):2931–2935, 2006.

[91] Marija Radmilovic-Radjenovic, Branislav Radjenovic, Matej Klas, Aleksandar Bojarov, and Stefan Matejcik. The breakdown mechanisms in electrical discharges: The role of the field emission effect in direct current discharges in microgaps. *Acta Physica Slovaca*, 63:105–205, 06 2013.

[92] H Ki Yasuda. *Plasma polymerization*. Academic press, 2012.

[93] Brian T Molnar and Jacob T Shelley. Modern plasma-based desorption/ionization: From atoms and molecules to chemical synthesis. *Mass Spectrometry Reviews*, 40(5):609–627, 2021.

[94] Andreas Schutze, James Y Jeong, Steven E Babayan, Jaeyoung Park, Gary S Selwyn, and Robert F Hicks. The atmospheric-pressure plasma jet: a review and comparison to other plasma sources. *IEEE transactions on plasma science*, 26(6):1685–1694, 1998.

[95] Gheorghe Dinescu and Eusebiu R Ionita. Radio frequency expanding plasmas at low, intermediate, and atmospheric pressure and their applications. *Pure and Applied Chemistry*, 80(9):1919–1930, 2008.

[96] Z Rahman, H Rahman, and A Rahman. Classification and generation of atmospheric pressure plasma and its principle applications. *Int. J. Math. Phys. Sci. Res*, 2:127–146, 2014.

[97] Peter J Bruggeman, Felipe Iza, and Ronny Brandenburg. Foundations of atmospheric pressure non-equilibrium plasmas. *Plasma Sources Science and Technology*, 26(12):123002, 2017.

[98] Jaeyoung Park, I Henins, HW Herrmann, GS Selwyn, JY Jeong, RF Hicks, D Shim, and CS Chang. An atmospheric pressure plasma source. *Applied Physics Letters*, 76(3):288–290, 2000.

[99] Claire Tendero, Christelle Tixier, Pascal Tristant, Jean Desmaison, and Philippe Leprince. Atmospheric pressure plasmas: A review. *Spectrochimica Acta Part B: Atomic Spectroscopy*, 61(1):2–30, 2006.

[100] Juergen F Kolb, A-A H Mohamed, Robert O Price, R James Swanson, Angela Bowman, Robert L Chiavarini, M Stacey, and KH Schoenbach. Cold atmospheric pressure air plasma jet for medical applications. *Applied Physics Letters*, 92(24):241501, 2008.

[101] Irina Velichko, Ivan Gordeev, Artem Shelemin, Daniil Nikitin, Jan Brinar, Pavel Pleskunov, Andrei Choukourov, Kateřina Pazder, and Josef Pulkrábek. Plasma jet and dielectric barrier discharge treatment of wheat seeds. *Plasma Chemistry and Plasma Processing*, 39:913–928, 2019.

[102] Michael Noeske, Jost Degenhardt, Silke Strudthoff, and Uwe Lommatzsch. Plasma jet treatment of five polymers at atmospheric pressure: surface modifications and the relevance for adhesion. *International journal of adhesion and adhesives*, 24(2):171–177, 2004.

[103] Chang-E Zhou and Chi-wai Kan. Plasma-assisted regenerable chitosan antimicrobial finishing for cotton. *Cellulose*, 21(4):2951–2962, 2014.

[104] C Chokradjaroen, X Wang, J Niu, T Fan, and N Saito. Fundamentals of solution plasma for advanced materials synthesis. *Materials Today Advances*, 14:100244, 2022.

[105] Naoki Shirai, Satoshi Uchida, and Fumiyoshi Tochikubo. Synthesis of metal nanoparticles by dual plasma electrolysis using atmospheric dc glow discharge in contact with liquid. *Japanese Journal of Applied Physics*, 53(4):046202, 2014.

[106] D Nikitin, A Choukourov, V Titov, L Kuzmicheva, I Lipatova, E Mezina, V Aleksandriiskii, A Shelemin, I Khalakhan, D Slavinska, et al. In situ coupling of chitosan onto polypropylene foils by an atmospheric pressure air glow discharge with a liquid cathode. *Carbohydrate polymers*, 154:30–39, 2016.

[107] PJ Bruggeman, Mark J Kushner, Bruce R Locke, Johannes GE Gardeniers, WG Graham, David B Graves, RCHM Hofman-Caris, Dragana Maric, Jonathan P Reid, Elisa Ceriani, et al. Plasma–liquid interactions: a review and roadmap. *Plasma sources science and technology*, 25(5):053002, 2016.

[108] Andrei Choukourov. Solution plasma processing of natural polymer-based materials. . , 62(7):4–30, 2019.

[109] X Lu, George V Naidis, Mounir Laroussi, Stephan Reuter, David B Graves, and Ken Ostrikov. Reactive species in non-equilibrium atmospheric-pressure plasmas: Generation, transport, and biological effects. *Physics Reports*, 630:1–84, 2016.

[110] AFH Van Gessel, KMJ Alards, and PJ Bruggeman. No production in an rf plasma jet at atmospheric pressure. *Journal of Physics D: Applied Physics*, 46(26):265202, 2013.

[111] BTJ Van Ham, S Hofmann, R Brandenburg, and Peter J Bruggeman. In situ absolute air, o3 and no densities in the effluent of a cold rf argon atmospheric pressure plasma jet obtained by molecular beam mass spectrometry. *Journal of Physics D: Applied Physics*, 47(22):224013, 2014.

[112] Seth A Norberg, Wei Tian, Eric Johnsen, and Mark J Kushner. Atmospheric pressure plasma jets interacting with liquid covered tissue: touching and not-touching the liquid. *Journal of Physics D: Applied Physics*, 47(47):475203, 2014.

[113] VS Santosh K Kondeti, Chi Q Phan, Kristian Wende, Helena Jablonowski, Urvashi Gangal, Jennifer L Granick, Ryan C Hunter, and Peter J Bruggeman. Long-lived and short-lived reactive species produced by a cold atmospheric pressure plasma jet for the inactivation of pseudomonas aeruginosa and staphylococcus aureus. *Free Radical Biology and Medicine*, 124:275–287, 2018.

[114] George Odian. *Principles of polymerization*. John Wiley & Sons, 2004.

[115] JM Tibbitt, R Jensen, AT Bell, and M Shen. A model for the kinetics of plasma polymerization. *Macromolecules*, 10(3):647–653, 1977.

[116] Hynek Biederman. *Plasma polymer films*. World Scientific, 2004.

[117] Dirk Willem Van Krevelen and Klaas Te Nijenhuis. *Properties of polymers: their correlation with chemical structure; their numerical estimation and prediction from additive group contributions*. Elsevier, 2009.

[118] Kateryna Bazaka, Mohan V Jacob, Russell J Crawford, and Elena P Ivanova. Plasma-assisted surface modification of organic biopolymers to prevent bacterial attachment. *Acta biomaterialia*, 7(5):2015–2028, 2011.

[119] Kalpani Y Perera, Jack Prendeville, Amit K Jaiswal, and Swarna Jaiswal. Cold plasma technology in food packaging. *Coatings*, 12(12):1896, 2022.

[120] T Tantiplapol, Y Singsawat, N Narongsil, S Damrongsakkul, N Saito, and I Prasertsung. Influences of solution plasma conditions on degradation rate and properties of chitosan. *Innovative Food Science & Emerging Technologies*, 32:116–120, 2015.

[121] Verena Jost, Karin Kobsik, Markus Schmid, and Klaus Noller. Influence of plasticiser on the barrier, mechanical and grease resistance properties of alginate cast films. *Carbohydrate polymers*, 110:309–319, 2014.

[122] Anyarat Watthanaphanit and Nagahiro Saito. Effect of polymer concentration on the depolymerization of sodium alginate by the solution plasma process. *Polymer degradation and stability*, 98(5):1072–1080, 2013.

[123] Luan Gustavo Santos, Gisele Fernanda Alves Silva, Bruno Marques Gomes, and Vilásia Guimarães Martins. A novel sodium alginate active films functionalized with purple onion peel extract (allium cepa). *Biocatalysis and Agricultural Biotechnology*, 35:102096, 2021.

[124] Jingxin Chen, Ankang Wu, Mingliang Yang, Yonghong Ge, Penta Pristijono, Jianrong Li, Baocheng Xu, and Hongbo Mi. Characterization of sodium alginate-based films incorporated with thymol for fresh-cut apple packaging. *Food Control*, 126:108063, 2021.

[125] I Prasertsung, S Damrongsakkul, C Terashima, N Saito, and O Takai. Preparation of low molecular weight chitosan using solution plasma system. *Carbohydrate Polymers*, 87(4):2745–2749, 2012.

[126] Nikolai V Tkachenko. *Optical spectroscopy: methods and instrumentations*. Elsevier, 2006.

[127] Hans-Joachim Kunze. *Introduction to plasma spectroscopy*, volume 56. Springer Science & Business Media, 2009.

[128] Herman L Wagner. The mark–houwink–sakurada equation for the viscosity of linear polyethylene. *Journal of physical and chemical reference data*, 14(2):611–617, 1985.

[129] Anita Martinsen, Gudmund Skjåk-Bræk, Olav Smidsrød, Flavio Zanetti, and Sergio Paoletti. Comparison of different methods for determination of molecular weight and molecular weight distribution of alginates. *Carbohydrate polymers*, 15(2):171–193, 1991.

[130] Wallace W Yau, Joseph J Kirkland, Donald D Bly, and Andre Striegel. *Modern size-exclusion liquid chromatography: practice of gel permeation and gel filtration chromatography*. John Wiley & Sons, 2009.

[131] R Silverstein. Spectroscopy chemistry nmr ftir ms (1962.). 3.

[132] James Keeler. *Understanding NMR spectroscopy*. John Wiley & Sons, 2010.

[133] Byung Yun Yang and Rex Montgomery. Degree of acetylation of heteropolysaccharides. *Carbohydrate Research*, 323(1-4):156–162, 1999.

[134] Asako Hirai, Hisashi Odani, and Akio Nakajima. Determination of degree of deacetylation of chitosan by 1 h nmr spectroscopy. *Polymer Bulletin*, 26:87–94, 1991.

[135] Douglas A Skoog, F James Holler, and Stanley R Crouch. *Principles of instrumental analysis*. Cengage learning, 2017.

[136] John C Lindon, George E Tranter, and David Koppenaal. *Encyclopedia of spectroscopy and spectrometry*. Academic Press, 2016.

[137] John Coates. Interpretation of infrared spectra, a practical approach, 2000.

[138] Anthony C Fischer-Cripps and DW Nicholson. Nanoindentation. mechanical engineering series. *Appl. Mech. Rev.*, 57(2):B12–B12, 2004.

[139] Dilara Konuk Takma and Figen Korel. Impact of preharvest and postharvest alginate treatments enriched with vanillin on postharvest decay, biochemical properties, quality and sensory attributes of table grapes. *Food chemistry*, 221:187–195, 2017.

[140] T Acsente, MD Ionita, M Teodorescu, V Marascu, and G Dinescu. Surface modification of polymethylmethacrylate foils using an atmospheric pressure plasma jet in presence of water vapors. *Thin Solid Films*, 614:25–30, 2016.

[141] Abdollah Sarani, Anton Yu Nikiforov, and Christophe Leys. Atmospheric pressure plasma jet in ar and ar/h 2 o mixtures: Optical emission spectroscopy and temperature measurements. *Physics of Plasmas*, 17(6):063504, 2010.

[142] A Yu Nikiforov, Abdollah Sarani, and Ch Leys. The influence of water vapor content on electrical and spectral properties of an atmospheric pressure plasma jet. *Plasma Sources Science and Technology*, 20(1):015014, 2011.

[143] Francesco Tampieri, Maria-Pau Ginebra, and Cristina Canal. Quantification of plasma-produced hydroxyl radicals in solution and their dependence on the ph. *Analytical chemistry*, 93(8):3666–3670, 2021.

[144] Naotsugu Nagasawa, Hiroshi Mitomo, Fumio Yoshii, and Tamikazu Kume. Radiation-induced degradation of sodium alginate. *Polymer Degradation and Stability*, 69(3):279–285, 2000.

[145] Zhengduo Wang, Qiang Chen, Yen Wei, Alexander A Fridman, Gregory Fridman, and Hai-Feng Ji. Chemistry of air, n 2, and o 2 reverse vortex gliding arc plasma system. *Plasma Medicine*, 9(1), 2019.

[146] Konstantin F Sergeichev, Natalya A Lukina, Ruslan M Sarimov, Igor G Smirnov, Alexander V Simakin, Aleksey S Dorokhov, and Sergey V Gudkov. Physicochemical properties of pure water treated by pure argon plasma jet generated by microwave discharge in opened atmosphere. *Frontiers in Physics*, 8:614684, 2021.

[147] Chu Dinh Kinh, Tran Vinh Thien, Tran Thai Hoa, and Dinh Quang Khieu. Interpretation of 1h-nmr spectrum of alginate by 1h-1h tocsy and cosy spectrum. *Vietnam Journal of Chemistry*, 45(6):772–772, 2007.

[148] AaGRS Penman and GR Sanderson. A method for the determination of uronic acid sequence in alginates. *Carbohydrate Research*, 25(2):273–282, 1972.

[149] Celine Sartori, Dudley S Finch, Brian Ralph, and Keith Gilding. Determination of the cation content of alginate thin films by fti. r. spectroscopy. *Polymer*, 38(1):43–51, 1997.

[150] Gabriela A Paula, Norma MB Benevides, Arcelina P Cunha, Ana Vitória de Oliveira, Alaídes MB Pinto, João Paulo S Morais, and Henriette MC Azeredo. Development and characterization of edible films from mixtures of κ-carrageenan, ι-carrageenan, and alginate. *Food Hydrocolloids*, 47:140–145, 2015.

[151] Gwen Lawrie, Imelda Keen, Barry Drew, Adrienne Chandler-Temple, Llewellyn Rintoul, Peter Fredericks, and Lisbeth Grøndahl. Interactions between alginate and chitosan biopolymers characterized using ftir and xps. *Biomacromolecules*, 8(8):2533–2541, 2007.

[152] Bishwa Chandra Adhikari, Pradeep Lamichhane, Jun Sup Lim, Linh N Nguyen, and Eun Ha Choi. Generation of reactive species by naturally sucked air in the ar plasma jet. *Results in Physics*, 30:104863, 2021.

[153] Mounir Ouzir, Sara El Bernoussi, Mohamed Tabyaoui, and Khalid Taghzouti. Almond oil: A comprehensive review of chemical composition, extraction methods, preservation conditions, potential health benefits, and safety. *Comprehensive reviews in food science and food safety*, 20(4):3344–3387, 2021.

[154] Milda E Embuscado and Kerry C Huber. *Edible films and coatings for food applications*, volume 9. Springer, 2009.

[155] GI Olivas, DS Mattinson, and GV Barbosa-Cánovas. Alginate coatings for preservation of minimally processed 'gala'apples. *Postharvest biology and Technology*, 45(1):89–96, 2007.

[156] Massimo Malerba and Raffaella Cerana. Chitosan effects on plant systems. *International journal of molecular sciences*, 17(7):996, 2016.

[157] A Khlyustova, N Sirotkin, I Naumova, A Tarasov, and V Titov. Solution plasma processing as an environmentally friendly method for low-molecular chitosan production. *Plasma Chemistry and Plasma Processing*, 42(3):587–603, 2022.

[158] Mohammad R Kasaai. Determination of the degree of n-acetylation for chitin and chitosan by various nmr spectroscopy techniques: A review. *Carbohydrate polymers*, 79(4):801–810, 2010.

[159] M Lavertu, Z Xia, AN Serreqi, M Berrada, A Rodrigues, D Wang, MD Buschmann, and Ajay Gupta. A validated 1h nmr method for the determination of the degree of deacetylation of chitosan. *Journal of pharmaceutical and biomedical analysis*, 32(6):1149–1158, 2003.

[160] Kenji Tomihata and Yoshito Ikada. In vitro and in vivo degradation of films of chitin and its deacetylated derivatives. *Biomaterials*, 18(7):567–575, 1997.

List of Figures

List of Tables